UNIVERSITÀ DEGLI STUDI DI PADOVA

DII - Department of Industrial Engineering

Master's course in Aerospace engineering

Design and assembly of a facility for kinematic testing of docking mechanisms

Supervisor: Francesco Branz

Student: Leonardo Dall'Est
2056506

Academic year 2023/2024

ABSTRACT

This thesis presents the process followed for the design and assembly of a kinematics test facility. The system was designed because the Space Systems Lab needed a new facility that was more rapid and practical than the one already in use. The work began with an analysis of kinematics simulators and their requirements, then with the study of the mechanism that the facility would test, and of the previous test procedures. Then, a set of requirements was defined. The available components were considered and some new necessary components were acquired. Finally, the system was designed and a preliminary analysis of potentially critical load configurations on components was performed. A program was written to control the system, and the test procedure was implemented. After the final assembly of the system, some test trials were conducted. Although the performance met the requirements, improvements could be made in the future.

SOMMARIO

In questa tesi è presentato il processo seguito per effettuare il design e l'assemblaggio di una facility per test cinematici. Questo sistema è stato progettato perchè il Laboratorio di Sistemi Spaziali necessitava una nuova apparecchiatura che fosse più rapida e pratica nel suo utilizzo rispetto a quella già presente. Il progetto è iniziato con un'analisi dei simulatori cinematici e dei loro requisiti, poi con lo studio del meccanismo che il sistema avrebbe testato, e dei test precedentemente effettuati. Poi, dei requisiti sono stati fissati. I componenti disponibili sono stati considerati e alcuni nuovi componenti sono stati acquisiti. In fine, il sistema è stato progettato e l'analisi di alcune condizioni di carico potenzialmente critiche è stato effettuato. Un programma è stato scritto per controllare il sistema e la procedura di test è stata implementata. Dopo l'assemblaggio finale del sistema, sono stati condotti alcuni test di prova. Benché le performance raggiungano i requisiti, alcuni miglioramenti possono essere effettuati nel futuro.

Contents

1 Introduction

As space operations in orbit gradually increase in complexity, the capabilities of the involved systems must meet the new and improved requirements. One of the systems that are slowly becoming more relevant is the docking mechanism, as it is a prerequisite for advanced operations between satellites such as maintenance, de-orbiting and debris removal. Consequently, the need to test this type of mechanism is gradually increasing while the market demands the production of new testing facilities, both dynamic and kinematic, to prove the new and improved mechanisms can meet the latest standards.

Since these facilities are improving their ease of use, they are allowing increasingly fast progress. They also must provide a fair degree of adaptability to various kinds of mechanisms, to reduce the lapse of time in which the facility remains non-operational.

It is with the necessity for this kind of simulator in the Space Systems Laboratory that this project started at *Università degli Studi di Padova*: the goal is to provide a simulator to test small mechanisms such as the DOCKS docking system [13]. The requirements for the aforementioned testing facility are:

- the ability to impose a known misalignment along x and y coordinates to the tested mechanism;
- the ability for the lower segment of the mechanism to freely move on the x-y plane;
- the possibility to measure the position of both upper and lower segments of the tested mechanism (this position needs to be possible to measure or already be known);
- a sufficient stiffness of the system to avoid flexing and consequently affecting measurements.

These requirements are carefully considered during the whole design phase of the project and are the main driving characteristic of the testing facility as a whole.

To present all these considerations this work is going to be separated into four main sections: *2. State of the Art*, *3. Design, models, and methods*, *4. Final assembly and testing*, *5. Conclusions*. The *State of the Art* section focuses on similar previously built mechanisms and similar tests conducted on both DOCKS and similar mechanisms. The *Design, models, and methods* section is the main body of this work, in which all the design steps and the building procedure are explained in detail. Next, the *Final assembly and testing* and *Conclusions* sections are quite self-explanatory: they will list the results that are possible to achieve with the built system and provide an understanding as to whether its performance meets the requirements mentioned above, while also expanding on which could be further improvements to the testing apparatus.

2 State of the Art

2.1 Spacecraft simulators

2.1.1 Introduction to spacecraft simulators

It is common for a satellite to perform some orbital manoeuvres while near other spacecraft or satellites, as it is common to have even interaction between them. Some examples of these manoeuvres are berthing, capturing, formation flight and the core subject of this thesis: docking.

These kinds of manoeuvres present one of the many critical moments during the operational lifespan of a satellite. They are therefore simulated both virtually and physically, through the use of computer software or test facilities.

While virtual testing may be sufficient for non-critical applications, in the case of components and systems that operate in the previously mentioned environment, the uncertainty that virtual simulations provide makes it necessary to prove that the designed components and systems can withstand the loads and perform the planned movements or tasks.

It is from this necessity that spacecraft simulators are born, to simulate an environment that comes as close as possible to the one in which the manoeuvres mentioned before take place.

As explained by Wilde et al. [8] the three main differences between the orbital and the terrestrial environment that affect proximity manoeuvres of spacecraft are:

- the relative movement present between the considered bodies caused by their different position in orbit (although the movement may be small it still needs to be accounted for);
- proximity manoeuvres typically occur in an environment that can be considered frictionless and therefore the dynamics of the objects are dominated by their in-

ertia. The objects are subsequently subject to various kinds of torques from the environment such as residual aerodynamic drag, magnetic field forces and gravitational pull from Earth, as well as from internal sources, such as actuators, jet thrusters and reaction wheels;

- the lighting conditions during spacecraft proximity manoeuvres are characterised by stark contrasts between light (the illuminated spacecraft from artificial sources or the sun) and shadow.

2.1.2 Spacecraft simulator types

The three characteristics just mentioned need to be carefully considered during the design, building and testing process of spacecraft simulators, as their correct implementation may be the difference between a trustworthy simulator and one that relays incorrect data, The degree to which the environment must be reproduced depends on the systems must be tested, therefore lowering the simulation requirements depending on the application.

In any case, depending on the kind of tests that must be conducted the simulators can be categorised into two types: dynamic and kinematic. In particular, kinematic simulators are systems where motion is imposed on the simulated spacecraft by using forces or torques applied by actuators, these torques are not representative of the actual set of forces that will be applied to the spacecraft during its mission. Consequently, kinematics simulators can only reproduce the kinematics and differential kinematics of the involved systems.

On the other hand, dynamics simulators are systems in which actuators and thrusters are present on board the simulated systems, therefore the loads applied to it closely resemble the ones to which the system is subject during its operational life. Another factor that differentiates dynamics simulators from kinematics is that the former implements methods of suspension that are used to isolate the simulated spacecraft from the

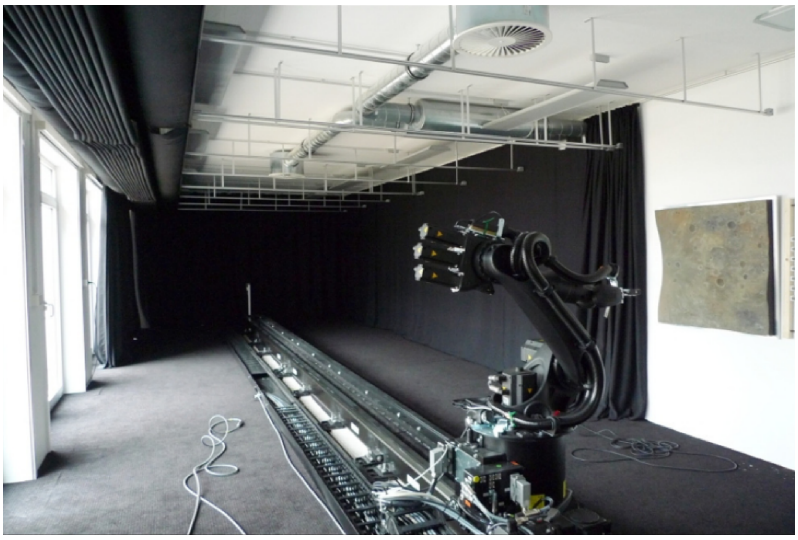

Figure 1: The DLR Testbed for Robotic Optical Navigation [3]

direct effects of gravity and some of the ground-reaction torques and forces. Therefore, although introducing a fair amount of complexity, dynamics simulators can simulate both the dynamics and the kinematics of the simulated vehicle (even if kinematics simulation is limited to some degree).

The two types of simulators are usually used for different reasons: commonly, kinematic simulators are used for research, development and testing of sensors and to provide data on their performance and navigation algorithms, while dynamics simulators are used for testing that involves actuators, more specifically their performance, contact dynamics, steering logic, the performance of docking and capture mechanisms. In the end, they can also be used for the verification of dynamic models for multi-body systems and testing of other whole-system performance characteristics.

2.1.3 Spacecraft simulator requirements

To better explain all the necessities of a spacecraft simulator, it is beneficial to separate them into two groups: primary and secondary requirements. The former are those requirements that must necessarily be met for the simulation to give meaningful results.

The secondary requirements are affected by all those factors outside the simulation requirements and have an impact on the time required for a successful testing campaign to be completed.

Primary requirements

As previously mentioned, primary requirements must be met to have meaningful results from the simulator, independently from the type of simulator. They are mechanics of the simulation, degrees of freedom of the simulator and number of simulated objects.

Mechanics of the simulation: Depending on the simulator type the requirements for its mechanics vary. For instance, dynamics simulators require that the simulated system interacts as little as possible with the environment, to not affect its dynamics. Hence, the motion of the vehicles must be controlled with actuators that are mounted on the vehicle itself and controlled by internal electronics and algorithms. Furthermore, all the power supplied to onboard systems must also be internally generated or available. To complete the mechanics requirements communication between the simulated vehicles and their environment must be achieved through wireless communications protocols. All these requirements make the simulation system very complex to operate and maintain. These complexities cause further difficulties when faced with the necessity to adapt the simulator to test new systems, as their design is typically focused on a single test subject.

On the other hand, kinematics simulators must be able to move test articles precisely along predefined trajectories or positions positions and orientations. Since the components and systems simulated with this type of simulator are often full-scale vehicles or very big parts, powerful actuators are required. This makes most kinematics simulators very rigid, which causes any contact between test vehicles during simulations to be potentially damaging to the vehicles and the simulator apparatus. Therefore, they often present shock absorbers or dampeners where such risk is particularly high. In this type of simulator, the actuators and onboard systems are usually controlled by external

computers and powered by external sources. As a result, the computing and power resources available are greater than those in dynamics simulators. This allows for the easy integration of individual test articles, which is advantageous for the prototyping of new components or technologies.

Degrees of freedom: they are the second primary characteristic of the simulation systems; this characteristic defines how many degrees of freedom (hereby DoF) the system has. This requirement affects the complexity of the system as at least one actuator and guide must be added for every DoF that is simulated. For a lot of applications, planar simulation systems are sufficient. These simulation systems usually offer 2 linear movements and a rotation perpendicular to the two movements. More advanced simulators add 2 DoF to the 3 that are already present by introducing the capability to rotate the simulated object around 2 additional axes. The addition of the last DoF to reach the complete 6 is achieved by adding the capability of the system to move along the axis perpendicular to the other two movement axes. Kinematics simulators often present 6 DoF while dynamics simulators are usually limited to two 3 with few exceptions.

Number of simulated objects: The third and last primary requirement is the number of controlled objects in the simulation. A dynamics simulator with only one simulated vehicle is adequate since as mentioned before this kind of simulator is usually used for testing actuator and their control algorithms. A kinematics simulator however can fulfil its objective of replicating the relative geometry of proximity manoeuvres by incorporating one stationary object and one actuated vehicle in the simulation. The count of actuated simulation vehicles can be increased to broaden the motion envelope of the simulation. This becomes essential for peculiar simulations of circumnavigations, capture/docking, or relative navigation of multiple bodies in satellite formations. For most kinematics simulators and hybrid simulators, the inclusion of simulation objects necessitates the addition of intricate positioning mechanisms. For conventional dynamics simulators, the individual vehicles are inherently self-sufficient, so the addition of simulation vehicles

does not require significant modifications to the simulation environment.

Secondary requirements

The secondary requirements for simulation systems are accessibility, availability and endurance. These parameters strongly affect the time employed to design a working system simulator and the time to conduct the testing on simulated objects.

Accessibilty: Accessibility is the measure that indicates the difficulty that would be encountered while swapping another vehicle for simulation or accessing the current simulated vehicle to make necessary improvements.

Availability: Availability measures how rapidly and conveniently the simulation system can be made ready for operation for testing purposes. This parameter, therefore, covers considerations such as organisation times and staff training.

Endurance: The endurance describes the length of time during which the system can continuously operate before refuelling or maintenance. Consequently, this parameter impacts the testing schedule and the overall timeline of the project, especially the length of the downtime between simulations. Luckily kinematics simulators have virtually unlimited endurance since their actuators are external as is computational power. For dynamic simulators, on the other hand, this parameter is very important since they have limited or even very limited endurance due to their nature, having onboard batteries and propellant tanks. Their operation time may also be limited by the microgravity conditions.

Robustness: This last parameter defines the capability of the system to endure impacts and loads due to simulation anomalies and the inherent nature of the conducted tests. This is especially true for kinematic systems, since usually this type of system operates with very big vehicles, involves high masses and the motion of the vehicles is generated through powerful motors and subsystems. This gives them a disadvantage when compared to dynamics systems, in which tested vehicles are usually smaller and

have subsequently also smaller inertia.

2.1.4 Spacecraft kinematics simulators

As discussed in the last paragraph the primary design difficulties for kinematics simulation systems are the number of simulated objects, the accuracy and precision of the simulation system and the number of degrees of freedom. While some simulators use robotics arms (like the one shown in *figure 1*) that grant all 6 DOF, most of them are Cartesian motion systems (*figure 2*) that use independent motion systems for each DOF. They can have anything from 1 to 6 DOF and frequently support one or two vehicles. The linear motion is usually achieved through tracks and/or suspension cables, while the rotatory motion is implemented through gimbals or pan-tilt mechanisms. The first one to be built was the NASA Rendezvous Docking Simulator (RDS) in Virginia. This was a hangar-sized facility, originally used for full-scale piloted and teleoperated docking simulations.

Similar large-scale Cartesian simulators have been built around the world, an example can be the Dynamic Overhead Target Simulator (DOTS)[1], which is one of the facilities that operate inside the Flight Robotics Laboratory (FLR) at the NASA Marshall Space Flight Center in Huntsville, Alabama. This kinematics simulator is an 8 DoF overhead gantry that provides the capability to withstand the weight of a 500lb payload. This system is fed with data obtained through inverse kinematics simulation of the required simulated movements that can be applied to both a chaser and a target satellite.

Some further examples of kinematics simulators are the Space Operations Simulation Center (SOSC) in Lockheed Martin or by the Japanese Aerospace Exploration Agency (JAXA) with Rendezvous and Docking Operation Test System (RDOTS) in Tsukuba Space Center.

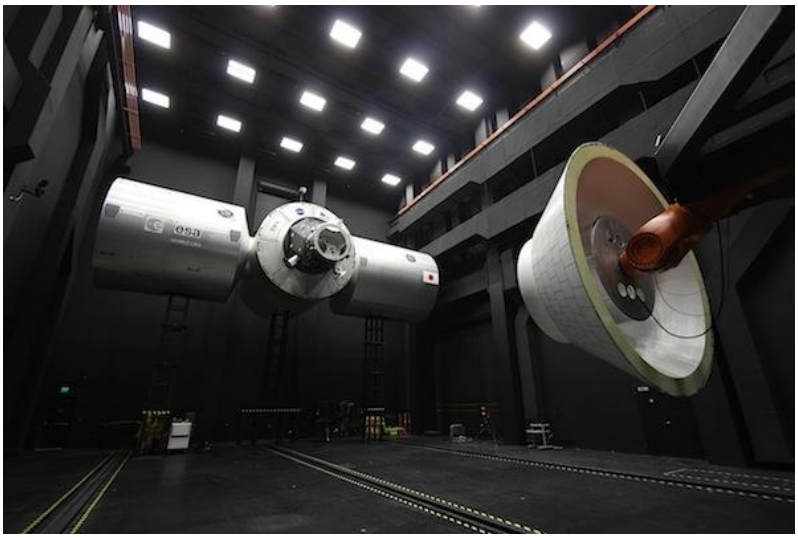

Figure 2: The Lockheed Martin SOSC kinematics simulator [4]

2.1.5 Spacecraft dynamics simulators

The primary design requirement for dynamics simulation systems is to make the dynamic interaction between the simulated vehicles and the environment as negligible as possible, for this requirement to be met the simulated vehicles must be self-contained. The availability and accessibility of the system depend on the type of class of the simulation system used in the project. Dynamics simulation systems present a wider variety of simulator classes when compared to kinematics simulators. The five main classes are: orbital micro-gravity systems, suborbital micro-gravity systems, neutral buoyancy facilities, air-bearing systems, and suspension systems.

Orbital micro-gravity systems: To achieve the ideal environment to test the dynamics of a system in space would be to put the test subject inside a pressurised container in orbit. This is exactly what this type of simulator achieves, but its price is prohibitive, for this reason only one simulator of this type exists: it's the SPHERES laboratory aboard the International Space Station (ISS)[2].

Suborbital micro-gravity systems: as an alternative to an orbital facility, they enable simulations with the full 6 DoF but only for periods that go from a few seconds to a few

minutes. This condition can be achieved through the use of:

- sounding rockets: through the use of a rocket the tested system is launched in a sub-orbital trajectory, providing after engine cut-off up to 20 minutes of $0g$ conditions
- drop towers and shafts: used more for experiments than for simulation can also provide near 0 gravity for brief periods (about 10 seconds)
- parabolic flights: the most used of the 3 since it enables personnel for test set-up and requires less automation, a plane performs a manoeuvre, such as a parabola, to provide near 0g condition during it.

Neutral-buoyancy facilities: They are large water tanks, for simulating micro-gravity by balancing buoyancy and the weight of the test subject, the interactions between objects and water make them feasible for only specific applications.

Air bearing systems: The most common method for dynamics simulators to decouple the environment and the tested object, they achieve near zero friction between the ground and the contact points of the simulated vehicle through the use of air cushions on these contact points. These types of facilities are categorized into passive floor/table systems, active floor/table systems, pitch and roll table systems for emulation of orbital relative acceleration, ABV design.

Suspension systems: they simulate micro-gravity by supporting components of space appendages such as joints. They are mainly used for testing robotic arms in micro-gravity or deploying mechanisms of various subsystems.

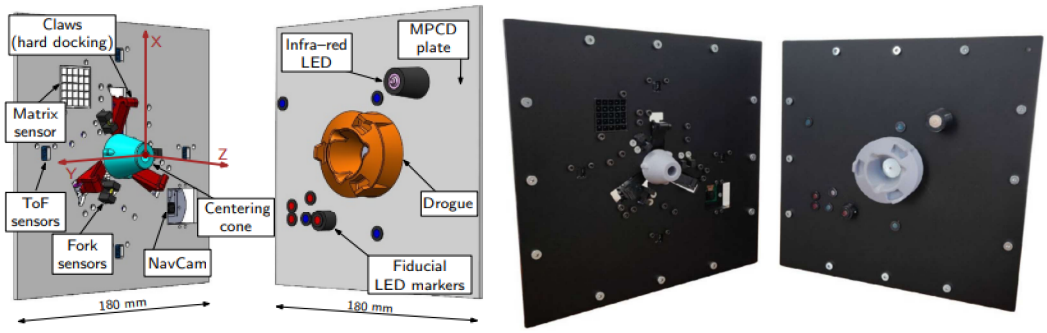

Figure 3: CAD and prototype of both DOCKS interfaces [13]

2.2 The DOCKS docking system

The mechanism that is going to be the main test subject of this thesis is going to be the DOCKS docking mechanism shown in *figure 3*. Therefore a brief description of what its components and features are is considered necessary.

2.2.1 Intro to DOCKS and its mission

As explained in the paper "Kinematic tests on a docking mechanism for microsatellites"[13] DOCKS will be one of the systems mounted aboard the Space Rider (SR) vehicle and to be more precise will be part of the Space Rider Observer Cube mission whose operations can be divided into five main phases, nominally:

1. Launch and early operation: SROC will be launched while housed inside SR and released in space through the use of a dedicated mechanism;

2. Commissioning and performance verification phase: capabilities for critical operations will be verified;

3. Proximity operation: SROC will perform observation cycles of SR from 300 to 5km distance;

4. Docking and retrieval: In this phase, SROC performs the final approach to SR,

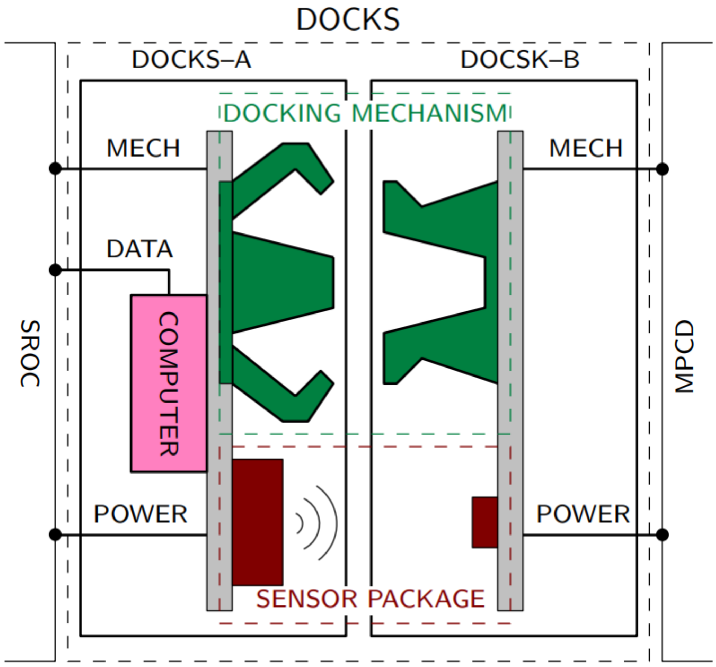

Figure 4: Schematics of DOCKS (A left, B right) [13]

docks with the Multi-Purpose CubeSat Dispenser (MCPD) and is retrieved inside SR.

5. End of mission: SROC re-enters Earth's atmosphere while aboard SR.

DOCKS will be one of the critical components in the 4th phase in virtue of being the docking mechanism as the sensors for alignment are mounted on it. The sensors will have to estimate the two objects' relative position and pose during the last phases of proximity operations and the docking mechanism is going to provide the rigid connection between the two vehicles for the rest of the mission. The design objectives of DOCKS were to create a standalone system able to manage the docking phase from ultra-close proximity (<1m) until a safe connection is achieved.

In *Figure 4* the scheme for the docking system is presented, on the right DOCKS-A can be seen while on the left DOCKS-B. DOCKS-A will be connected to SROC (chaser

satellite) via mechanical, power and data interfaces; DOCKS-A is defined as the 'smart' part of DOCKS since all of the sensors and computational capabilities of the system are mounted on it. Meanwhile, DOCKS-B is completely passive, making the overall system more ductile for future applications that may or may not have the same requirements.

2.2.2 The sensor suite

The sensor suite mounted on DOCKS-A has the objective of retrieving the relative pose of the target in the last metre. It is composed of 3 types of sensors:

1. Navigation Camera (NavCam);
2. Four Time of Flight sensors (ToF) distance sensors;
3. Sensor for very close proximity pose estimation.

Each of these sensors covers a different range of measurement and is fundamentally different from each other. Their ranges are designed so that they overlap with each other to avoid any period in which the pose of the SROC CubeSat cannot be estimated. Their resective ranges of operations can be seen in *figure 5*. The NavCam (a Raspberry Pi Camera Module V2.1) is employed between 1m and 80mm and can be used to estimate the complete pose of the target through a pattern of fiducial LED markers. The ToF sensors are used to retrieve the relative distance between the chaser and the target and the relative rotations of the target around the x and y axes. In the end, the sensor for estimating the pose during the last few millimetres is made from two parts: a 5 x 5 array of photo-transistors with a mask in the shape of a grid mounted on DOCKS-A and an infrared LED mounted on DOCKS-B. Depending on the distance and orientation of DOCKS-A concerning DOCKS-B the LED casts activates a different set of transistors. Based on which and how many transistors get activated it is possible to obtain the relative pose between the two objects. DOCKS-A also presents three fork sensors but they

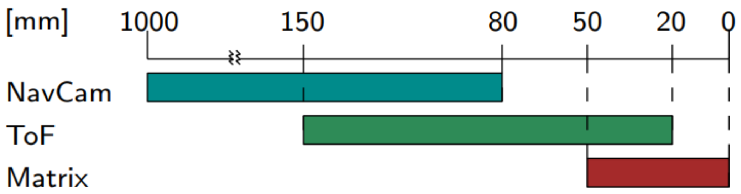

Figure 5: Ranges covered by each sensor during approach [13]

are not included in the sensor suite since they don't help in the estimation of the pose of the target but only act as a signal for a successful soft-docking.

2.2.3 The Docking mechanism

The core of DOCKS is the docking mechanism. Its function is to provide a rigid connection between the target and the chaser as well as to manage any misalignment caused by the limitation of the Guidance, Navigation, and Control system (GNC). Therefore, the docking mechanism needs to meet the following requirements:

- to provide a rigid connection between the target and the chaser;
- to provide multiple locking mechanisms that can be operated independently thus creating redundancy;
- to be compact as to fit inside a 0.5 CubeSat volume;
- to not contain any sliding mechanism to avoid wear and the risk of jams;
- to be axial-symmetric to allow easier integration in the bus, and not exceed a circular planar envelope of diameter 100mm;
- to provide self-centring capabilities and be able to tolerate misalignment of ± 8mm along x and y, an angular misalignment of ± 3deg around x and y and of ± 6deg around z;
- to provide magnetic soft-docking capabilities and grant a holding force of 5N.

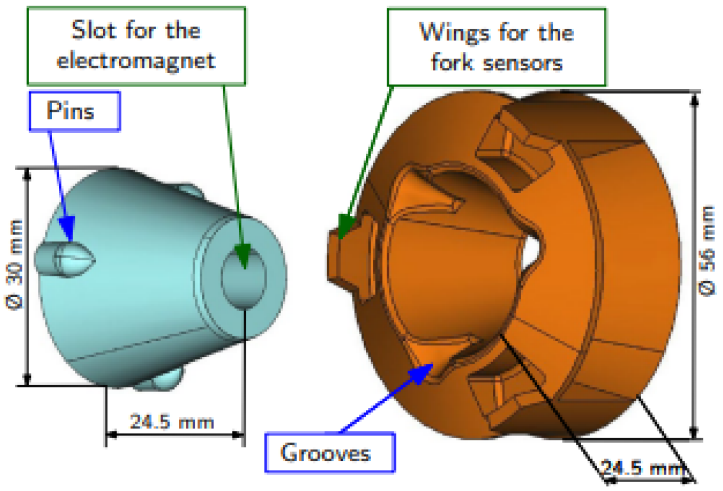

Figure 6: The probe-drogue mechanism up close [13]

To meet all these requirements, DOCKS combines a probe-drogue design (*figure 6*) with a gripper-like locking mechanism. The conic shape of both DOCKS-A and DOCKS-B causes the correction of any possible misalignments along and/or around x and y. DOCKS-A presents some pins on the probe, which produce self-alignment in the case of a rotation around the z-axis (the axial-symmetry axis). Each of these pins has its corresponding groove on DOCKS-B to create the necessary torque to make both DOCKS segments, and therefore their connected modules aligned. The soft-docking is the establishment of a non-rigid connection between the two parts. It is achieved through an electromagnet mounted on DOCKS-A that meets its ferromagnetic counterpart on DOCKS-B. When contact is established, the electromagnet is activated to create the soft-docking condition and to reduce the risk of bouncing after contact.

To obtain a rigid connection as imposed by the requirements, three claws are installed around the centring cone on DOCKS-A, equally spaced by 120° from each other. The hard docking is achieved when all three claws are closed along the drogue.

Each claw is connected to a four-bar linkage actuated by servo motors to avoid sliding contacts in the mechanism as required. The overall design of the drogue mechanism al-

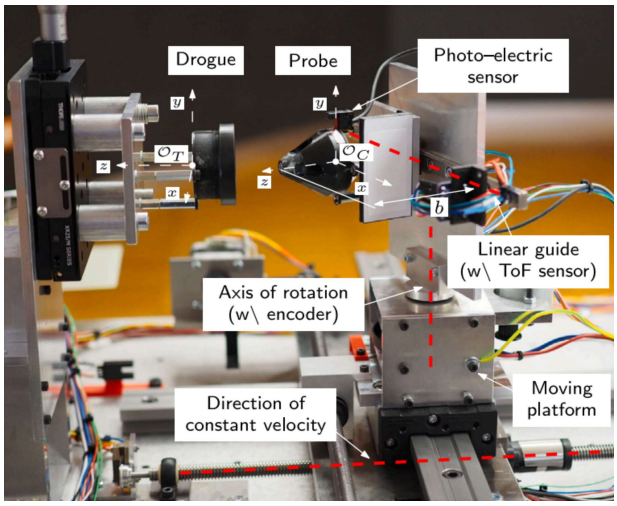

Figure 7: Setup used in "Miniature docking mechanism for CubeSats" [9]

lows for the management of misalignment along the z-axis of about 3mm. In other words if for some reason the probe is not already fully in contact with the drogue, a distance of up to 3mm can be handled by the clasping system, and the rigid connection between the two systems that house DOCKS-A and B can still be achieved. This condition may present in the case of malfunctioning of some other system such as the electromagnet during soft-docking.

2.3 Experimental kinematic validation of docking systems

A kinematic test of such a critical mechanism is necessary and valuable to properly characterize the docking mechanism as a device working on its own. It is particularly critical to evaluate its behaviour when presented with misalignments. As an example, while considering the test setup for a different mechanism in [9], the experiment neglects the effects of forces and focuses on the maximum theoretical misalignment that the mechanical system can handle.

The setup (*figure 7*) is built like the Cartesian kinematics simulator mentioned in subsection 2.1 but of reduced scale. It presents 3 DoF: translation along the z and

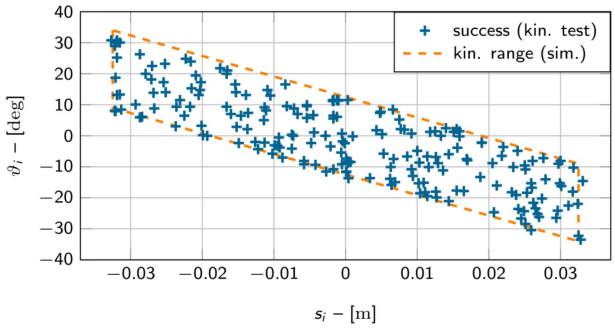

Figure 8: Simulation and experimental results compared [9]

x-axis; and rotation about the y-axis (since the system discussed in the paper is axial-symmetrical, rotation of the x-axis would be superfluous).

The drogue is fixed to the laboratory table, while a fixed speed v_z is applied to the part of the system that has a drogue mounted on it through the use of a stepper motor. The latter part of the system presents a linear guide and an axis of rotation in which movement is free.

During tests linear s and angular θ misalignments are manually imposed on the probe and measured with a Time-of-Flight (ToF) distance sensor. The full insertion of the probe into the drogue marks the end of the test, measured through a photo-electric sensor. One set of results obtained through this procedure can be seen in *figure 8*.

Another example of kinematic tests of docking mechanisms is found in Lion et. al [13], on the DOCKS docking system. The test setup is more complex when compared to the previous one since the movement is provided by a robotic arm with 6 DoF, and measures are taken using a 4-camera motion capture system that is focused on the workspace of the robotic arm.

During testing, DOCKS-A is rigidly connected to the robotic arm, while, depending on the test performed, DOCKS-B has different configurations (*figure 9*). One example of such configurations is having 5 DoF of the robotic arm locked while DOCKS-B is mounted on a linear rail that is free to move along the y-axis to test misalignments along said axis. Another type of test is the roll self-alignment test, during which DOCKS-B is

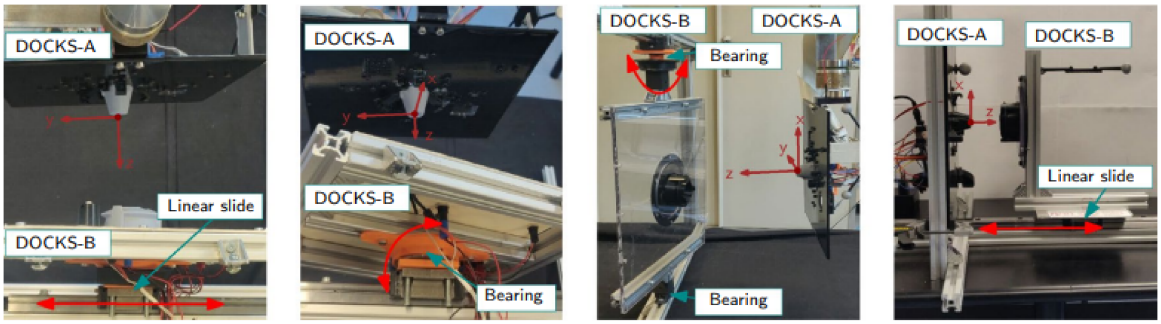

Figure 9: Various configurations of docking procedures [13]

connected to the supporting structure through a ball bearing that allows rotation about the z-axis. To test the other angular misalignments, DOCKS-B is mounted on a support which is connected to an external structure through two bearings which pass along the symmetry plane of the DOCKS-B plate, and enable a rotation similar to the one along the x-axis (although it introduces a slight misalignment). Being that the DOCKS system is symmetrical, tests for yaw and pitch misalignments are expected to give equivalent results. The last kind of test is performed along the z-axis. In this case, DOCKS-A is rigidly connected to the structure, while DOCKS-B is fixed on a linear rail and is free to move along the z-axis.

To better understand the following procedure a brief explanation of the reference system is in order. The tip of the probe at its axis of symmetry is the origin of the reference frame, where the z-axis points away from DOCKS-A and towards DOCKS-B. The x and y-axis complete the reference system. The test is conducted only after a 'zeroing' procedure. Since the procedure is very similar to the ones carried out after it, all of them will be explained in the following paragraph together. The peculiarity of this procedure is that it is used to align DOCKS-A with DOCKS-B. The two parts are connected without any misalignments and when hard-docking has been achieved the position of the robotic arm is saved as its zero position and the capture system is calibrated.

Following this procedure the tests are similar to each other and proceed as follows:

1. DOCKS-A is positioned 50mm away from the 'zero' position in the z direction;

2. a small misalignment is imposed to DOCKS-B, and measured by the motion capture system;

3. the robotic arm drives DOCKS-A with a straight trajectory towards DOCKS-B with a constant linear velocity;

4. once the parts are aligned, the fork sensor provides the confirmation signal and the claws are activated;

5. If the test run is successful, it is repeated with a variation of the misalignment by a fixed step. In case of failure, the misalignment is reduced by half the fixed-step.

A successful test is defined by the complete insertion of DOCKS-A inside DOCKS-B. By following the procedure the maximum acceptable value of misalignment is found. For each test, multiple runs were conducted to verify the result's repeatability, while the misalignment was extrapolated through the post-processing of the data acquired through the tracking system. The results are shown in *Figure 10* and the measured behaviour aligns with the expected behaviour.

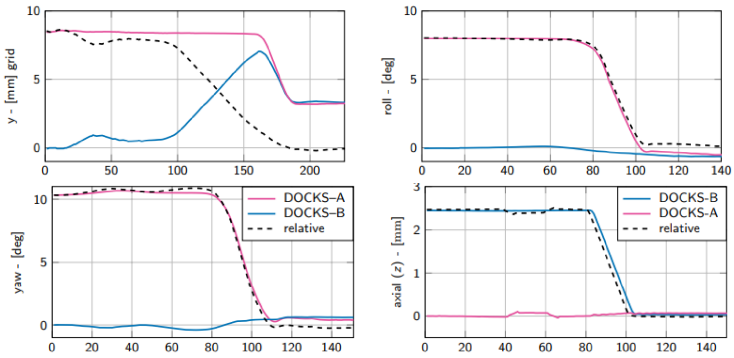

Figure 10: Test results for maximum misalignments for different test configurations [13]

3 Design, models and methods

Taking into consideration that the objective of this thesis is to build a facility for kinematic testing of docking mechanisms, it is possible to take as an example the simulators presented in section 2.1.4. As was discussed kinematic simulators allow up to the full 6 degrees of freedom of movement, but depending on the type of experiment that has to be conducted, the number of simulated DoF can be reduced even to 3.

Although both Cartesian simulators and robotic simulators can achieve all 6 DoF and some of the DoF can be limited depending on the type of experimentation to be conducted, the first presents a big advantage when considering the control algorithms, since every motor controls the movement independently. Furthermore, a Cartesian simulator setup procedure is simple and rapid, making the testing procedure require less time. Taking this into consideration, the facility discussed is going to be built using Cartesian kinematics simulators as a reference model, while reducing their dimensions since most of them are roughly the size of a building and the target mechanisms for the simulator built for this thesis are substantially smaller.

It would be ideal to retain all of the 6 degrees of freedom that this type of simulator could provide. However, considering the small volume of the apparatuses that will be tested, the simplicity required in the operation, and the size of the facility itself, some of these DoFs must be sacrificed. The two degrees of freedom in question will be the two rotations around the x and y-axis.

It is now needed to expand upon the requirements mentioned in the introduction section, briefly explaining why every requirement is needed and how it is met. Every component and mechanism will be discussed more in-depth later.

Ability to impose a known misalignment

This ability will be provided through the use of a set of electric stepper motors, which are connected to pulleys that are themselves attached to the mobile structure. The

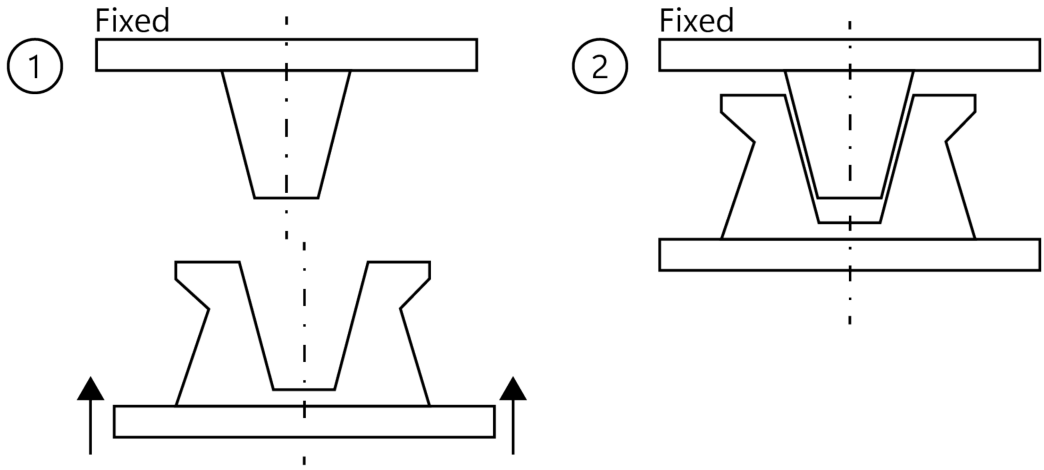

Figure 11: Movement that needs to be performed by the docking mechanism

precision of said movement is to be under 0.5mm to provide a fair amount of accuracy for testing small mechanisms. This is because the mechanisms that will be tested in the facility as seen previously in section 2.2.3 are going to have tolerance misalignment in the order of millimetres. Therefore the possibility of performing movements under the millimetre is required.

Free movement of the lower segment of the tested mechanism

The requirement of free movement of the lower part is going to be met by the use of a series of mini-ball transfer units. This allows the lower part of the mechanism to slide with very limited friction on the x-y plane as shown in *figure 11*, which is a requisite for the successful simulation of the docking procedure.

Measurement of positions

For the successful testing of the mechanism, it's imperative for the positions of both the lower and the upper segments of the mechanisms to be known. It would be possible to track the position of the upper mechanism by simply knowing how much movement has been imposed on it with a stepper motor. Unfortunately, the same cannot be said

for the lower one since it is able to move freely. The most important measure that needs to be taken during tests is the relative position of the two parts of the mechanism. In order to be able to measure this position, markers are applied on a removable structure connected to the DOCKS-B (or A) plate; their distance relative to the relevant parts of the mechanism is known. A set of 4 infrared tracking cameras is used to emit infrared light, which reflects on the markers. The camera picks up the reflection of said markers and triangulates their position. After this, post-processing of the collected data is required to extrapolate the actual position of the two parts.

Stiffness

The last requirement of the system is stiffness. Stiffness is needed to avoid the deformation of the testing apparatus during contact between DOCKS-A and DOCKS-B and therefore compromising the measurements of the two elements' positions. Stiffness is also necessary for the movement to be linear and repeatable. It is achieved through the use of multiple stainless steel guidance rods for the various moving elements of the system (at least two guides for each movement are present).

It is now possible to discuss how the system was designed and built while also considering these requirements.

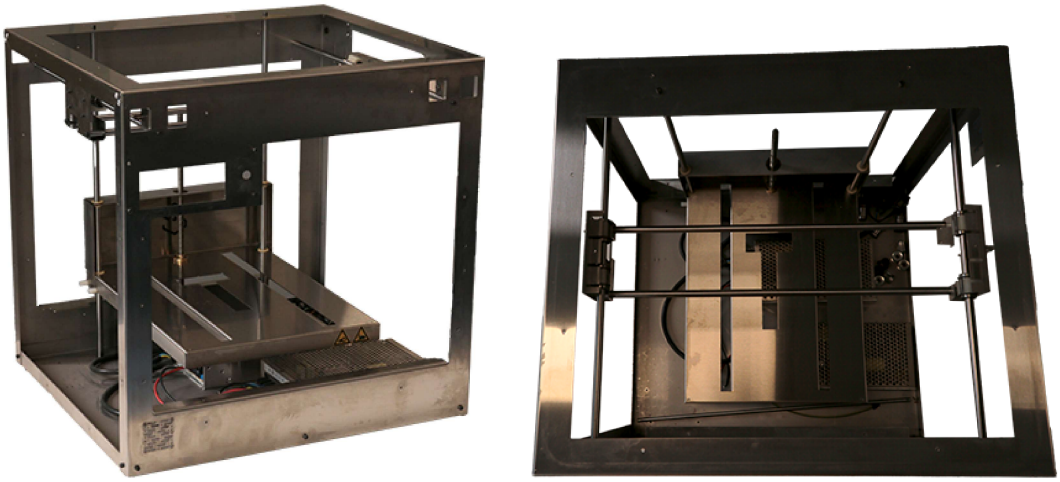

Figure 12: Kinematic test facility base structure with guides, side and top view

3.1 Structure and movements

Since the kinematics testing apparatus has previously been chosen to be of the Cartesian type, it is possible to take note of how previous systems were built in "Historical survey of kinematic and dynamic spacecraft simulators for laboratory experimentation of on-orbit proximity manoeuvres"[8]. It can be observed how most Cartesian simulators operate in a box-shaped environment, for instance in a building, to give some solid connections for the guides for the moving mechanisms. Having considered this, it makes sense for a smaller system to still use a box-shaped structure although smaller in dimensions. For this reason, an available 3D printer has been chosen as a starting structure (*figure 12*). It provides a rigid stainless steel structure in an almost cubic shape which is ideal for the type of movements that are going to be implemented. Furthermore, the structure already provides stainless steel rods of diameter 8mm that are solidly anchored through the use of M3 screws. They will act as the guides for the main movements of the kinematic test system, greatly simplifying the design process but also limiting it to the dimensions of the pre-existing structure.

The movements that the pre-existing structure and its guides can achieve are divided

Figure 13: Sleds components that support x-axis rods and motors

between two parts of the system: the lower and the upper part.

The former moves a platform that once housed the heated bed of the 3D printer. This part is only involved in the z-axis movement of the system through a leadscrew and is guided by two rods that pass through its back plate. This segment of the structure will house the part of the simulated mechanism that will be allowed to move freely. This is required for it to adapt to the other part of the mechanism.

The upper part of the mechanism is more complex and allows some movement along the x and y direction, which is achieved through a toothed pulley system that acts differently depending on which axis is considered.

Two rods are connected to the structure and provide anchoring points and guidance for the two sleds (*figure 13*) that support the two guidance rods themselves. The first two rods are fixed to the structure through the use of M3 screws and define the direction of the y-axis.

The sleds are made from a stainless steel plate that has been cut and bent to the desired shape. The two sleds are similar to each other since they both have the objective of providing a solid anchoring point for two guiding rods and housing the bearings through which the sleds are going to be able to slide on the two guidance rods mentioned in the previous paragraph. Although similar these sleds differ from each other, one is simpler and only has to fulfil the tasks just mentioned while the other has other additional objectives: to provide an anchoring point for the motor that is going to move

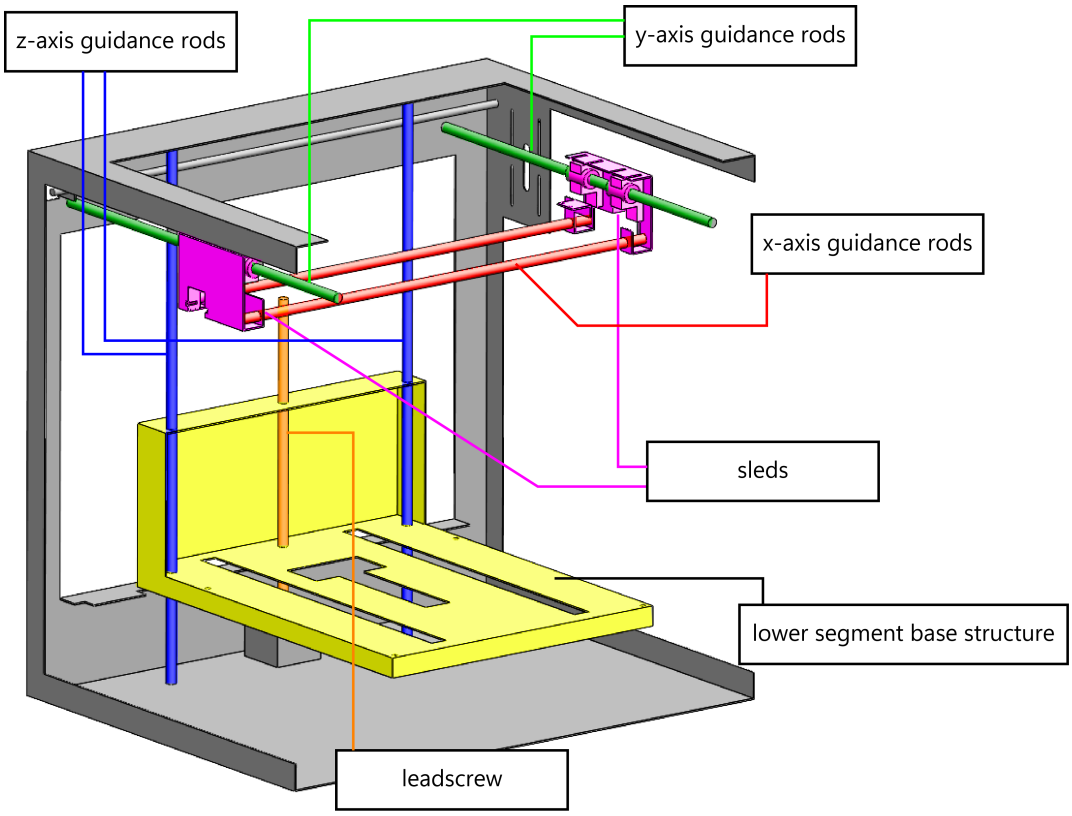

Figure 14: CAD representation of the pre-existing structure

the system along the x-axis and to house the limit switches for the x and y directions.

The last two rods that guide the movement of the upper part of the system define the direction of the x-axis and support the extruder mechanism and the hot end of the 3D printer that has been removed. The new supporting components for the new system are going to be explained in the following sections.

All of the elements present in this section have been observed and measured carefully and have been reproduced in the SolidWorks 3D CAD environment to assist in the design of the additional components that are going to be needed to build the kinematic simulator (*figure 14*).

3.2 Components and their operation

Now that the structure and its possible movements have been explained, it is possible to discuss which are the components that are going to drive said movements.

As seen in the *State of the Art* for kinematics simulators, powerful motors are used to control the position of the simulated vehicle. Taking this into consideration the stepper motors already present in the 3D printer have been repurposed for this project since they provide enough torque and precision for the required application. Furthermore, stepper motors are fairly simple and easy to control. In fact they can be managed directly from circuit boards, making them ideal for open-loop position control, which is how they are going to be used in this project.

3.2.1 Actuators

The actuators of the kinematics testing facility will be the stepper motors that were already in use by the 3D printer that can be seen in *figure 15*. They are 2 Moon's stepping motor 17HD4063-13N and one 17HD4063-18N. The first two are lower power motors that are going to be employed for the movement of the system along the x and y-axis, the second type of motor has a leadscrew substituting the normal motor shaft and is going move the lower segment of the system along the z-axis. The first two are going to be powered at 6V with a current of 0.65A while the second at 6V and 0.2A.

These stepper motors are hybrid stepper motors and have an angular resolution of 1,8°. As explained in [7] this type of motor has a stator with 8 poles, each of them with five teeth and with a coil around it to magnetize it. The rotor has 2 steel end-caps, each with 50 teeth that are separated by a permanent magnet.

The poles of the stator are spaced so that the teeth of two consecutive poles have different alignments from the stator teeth by 1.8 degrees. The permanent magnet in between the two plates is axially magnetized to have one steel end-cap that has N polarity while the other has S polarity. When no current is supplied to the motor the only

Figure 15: Stepper motors utilized in the kinematic test facility

magnetic flux present inside the motor is the one supplied by the permanent magnet, flowing axially from the N cap to the stator poles and returning to the magnet through the air gap at the S-polarized end cap. If the offset between the teeth of the stator wasn't present an equilibrium condition would be created, but, since this is not the case, this stability position is almost completely removed and the rotor can spin almost freely.

Nevertheless, a small alignment torque remains. However, this can be considered a positive feature of the motor. Even if it is not powered, the torque keeps the motor from rotating due to small forces that may act on the components connected to it. It prevents the last imposed position from being lost and therefore having to perform a homing procedure to precisely know the current position of the actuated component.

To operate a stepper motor the winding of the poles needs to be activated one at a time with a positive or negative current. The order in which the poles are energized to make the motor spin is +A, -B, -A, +B, +A to obtain a clockwise rotation, and vice versa for counter-clockwise rotation. This mode of operation is called full-step mode and is the simplest way of operating a stepper motor. Alternative methods of motor control are half-step and micro-stepping. These control modes differ from full-step in the timings of activation of the motor and the intensity of the current that is allowed to reach the motor windings. The phases used in the mentioned modes can be seen in *figure 16*.

Although there are some advantages to using full-step (or single-step) mode, nom-

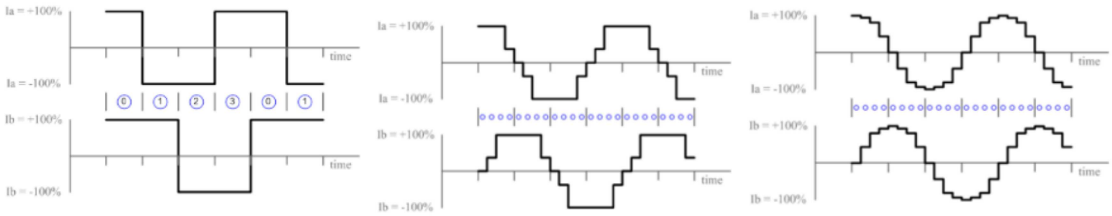

Figure 16: Stepper motor currents in different control modes [5]

inally, simplicity of control implementation and highest torque, it is not the most used control mode. Half-step and micro-step modes both have the disadvantage of reducing torque but improving the minimum rotation that the motor can produce, therefore improving its accuracy, doubling it for half-step mode and increasing it up to hundreds of times more in the case of micro-step mode. Therefore when more torque is needed or the dynamics of the system as a whole are more important half-step mode is utilized, while when increased precision is required micro-stepping is the go-to choice.

3.2.2 Sensors

As described in the last subsection stepper motors are usually used in systems where control is achieved through an open loop controller. This means that the control system is not affected by its output in any way. The type of control that is going to be used in the designed system is not different from it.

Considering that stepper motors are not capable of providing the position of the upper part of the system by themselves, some other kind of sensor must be employed. Since the movement of the stepper motor is discrete, it is possible to predict the position of the actuated mechanism only based on the input given to the motors. However, it is impossible to know the starting position of the actuated mechanism. This is where mechanical end-stops come into play: they are the simplest sensors that can deliver information on the current position of the system.

Mechanical end stops have as only output the tension at which they are powered

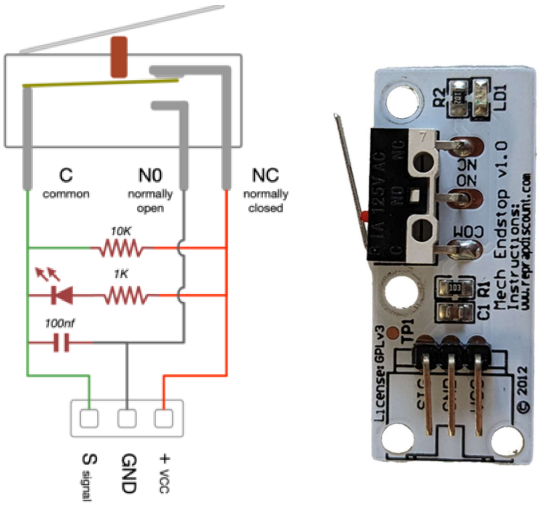

Figure 17: Endswitch used and its schematic [10]

and are very simple sensors. They are just switches that get activated when a force is applied to a mechanical lever that sticks out of the switch enclosure. They can be equipped with normally closed and/or normally open switches, both of which can be present at the same time on a single switch, giving the choice to the user of which mode to use. Normally closed switches are usually preferred since they provide additional safety in the case of the cables becoming disconnected from the switch. This is because the output when the cable disconnects is the same as when the switch is activated. Both of these cases would lead the system to stop and cease to operate.

This kind of switch comes with its flaws, nominally, the limited number of on/off cycles due to wear and tear, although most switches of this type are rated for well over one million cycles; they need a way to be mounted to the structure; the repeatability of the activation of the switch. All the flaws do not influence the operation of the kinematic test system, and it is for this reason that this switch is employed. The number of cycles that the switch is going to be subjected to is limited. A mounting structure for these components is already present or anyway easy to design and manufacture with a 3D printer, and the repeatability limitation does not concern the designed system

Figure 18: Some of the linear bearings used in the system, an example of linear guide [14]

since it only causes a mild difference after the centring phase but does not influence measurements.

The mechanical switches used in the system are based on MakerBot design and came with the 3D printer. They have the same schematic of the switch represented in *figure 17* and present an LED that indicates the correct operation of the switch (when the switch is activated the LED turns on).

3.2.3 Friction reduction

While the facility operates various movements will be imposed to the tested mechanism. This movements will take place by following the guides that define the movement along the x and y axis. To make the system move as smoothly as possible while maintaining x and y-axis alignment some linear bearings are used. They avoid the possibility excessively straining motors during operation that may cause steps to be skipped and the position of the mechanism to be lost. They reduce vibrations in the system since, as discussed later, the lower part of the system is particularly susceptible to it.

To remove friction the original system used linear ball bearings for rods of 8mm in diameter, which are housed inside some polymer holders that had to be removed as they would have been too bulky to use inside the system.

All the elements that connect to the guide use at least two linear ball bearings to

avoid any misalignment of the connected component to the rail caused by any slack in the bearing/rod/part coupling, and due to forces that may be applied to the components during tests.

On the lower segment of the system, these bearings are not present as they are not necessary. The system is powered by a more powerful motor along the z-axis and the linear motion of the lower segment of the mechanism is achieved through a leadscrew, which is a system that introduces friction itself.

The rods that act as guides on this part of the mechanism are simply run through a hole in the heat bed holder structure plates that are covered in plastic to avoid friction, but most importantly, to avoid wear of the guidance rod on the aluminium plate (this can be seen in *figure 14*). These rods assist in aligning the vertical path of the bed during operation and avoid the rotation of the bed structure when the motor for the z movement is activated.

While originally this segment of the system did not present any component for longitudinal movement it is now imposed from the requirement that the lower part of the mechanism has to be able to freely move on the horizontal plane.

There were different ways to achieve the free movement of the lower part of the tested mechanism, one of such ways would have been to use a low friction linear guide such as one shown in *figure 18*. This solution was discarded for the excessive amount of space it would occupy.

An additional requirement to the one of planar movement is the possibility for the part of the tested mechanism that is able to freely move to also rotate around the z axis.

This is why the 11MI-06-15 ball transfer units from ALWAYSE that are shown in *figure 19* have been chosen. The system as a whole will be connected to a rigid plate that is going to slide on top of the ball transfer units. This limits the interaction of the lower segment of the mechanism with the environment as much as possible, as its only contact points with the rest of the system will be the tip of the spheres. The spheres are made

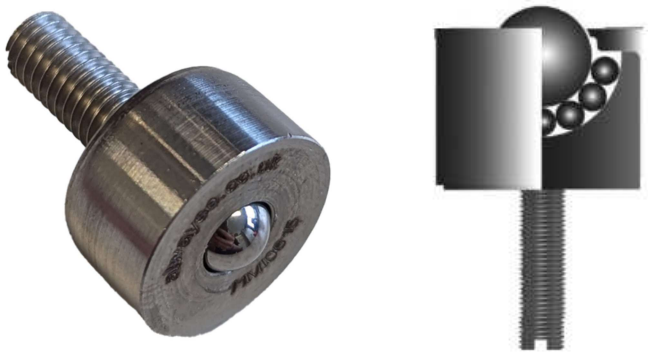

Figure 19: Ball transfer units used in the lower segment of the system

of stainless steel to avoid corrosion and wear, they can rotate while supported by other smaller steel spheres to further limit the amount of friction that the supported element is subject to. The plate on which the tested mechanism will be connected and that is going to make contact with the spheres is going to be made of polycarbonate and its design is going to be discussed in the next chapter.

3.2.4 Power components

To provide energy to the system as a whole a constant power supply is necessary. These power supplies are EPR 150-12 (*figure 20*). Both power supplies are powered by a standard 220V 2A power from standard power plugs and output up to 12.5A at 12V for a total power of 150W. Since these power supplies were meant for a 3D printer with various power-hungry components such as the heated bed and the extruder hot end, it is reasonable to be able to reduce the number of power supplies used from two to one since the maximum power draw that we can expect from our system is about 10W for each motor, for a maximum total power draw of about 30W.

The power supply delivered current directly to the previously installed control board. Conversion from 12V to the required voltage for each subsystem of the previous appli-

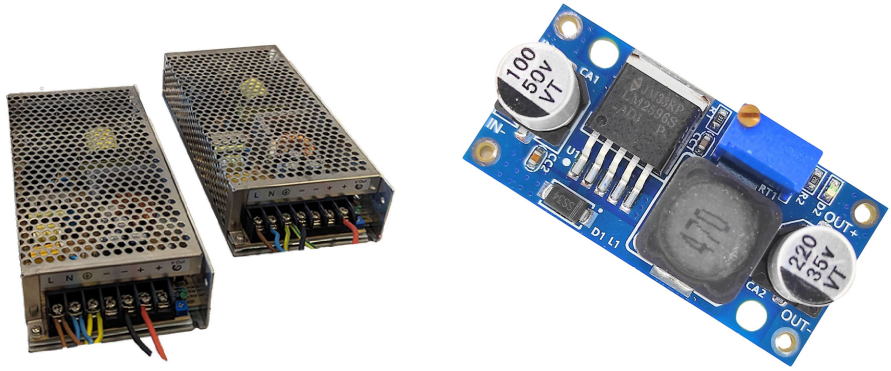

Figure 20: EPR 150-12 power supply and buck converter

cation happened on board so no other component was required. Alas, the same is not valid for our application and it is therefore necessary to reduce the voltage delivered from the power supply to the one at which the motors operate. This is achieved through the use of a buck converter(*figure 20*), which is a component which is composed of a switch that is controlled by a PWM algorithm, a diode and an inductance.

3.2.5 Movement transmission

Since both the actuators and the elements that are going to allow the movement of the system have been presented, the component that connects the actuators to the moved system is going to be discussed. The transmission of movement is achieved through the use of a toothed pulley-belt system.

These pulleys are characterized by having 16 teeth. They come pre-installed on the motors that control the movement along the x and y-axis. To transmit movement the motor that controls the movement along the x-axis is anchored on the sleds that support the guidance rods and is directly connected to the pulley that is itself fixed to the actuated part of the system through a screw and a washer on multiple points. The movement transmission on the y-axis is more complex, this is because the movement

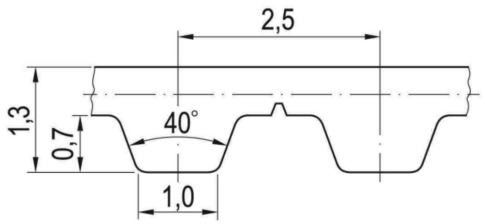

Figure 21: T 2,5 belt characteristics from catalogue [6]

needs to be transmitted to both sleds in the same way. The lack of compliance with this requirement would cause one of the two sleds to be dragged by the movement of the other. But since the guidance structure present some slack to compensate for the small misalignment caused by the manufacturing processes of the sleds, the dragging of one of the sleds from the other causes the the overall structure to warp and the change of the orientation of the x-axis. This is unacceptable for both the previous and current application and therefore both sleds are driven with the use of the belt pulley system. To have both sleds moving synchronously the stepper motor that drives the movement along the y-axis is connected through a belt and two pulleys to a small diameter shaft. This shaft transmits the rotation to two additional pulleys that move the belts that are themselves connected to the sleds.

The belts that were already present in the previous system had to be substituted for new ones of the same type and measured because of wear and ageing to guarantee the best possible performance. The substitute belts have the same characteristics as the previously used ones and are four 6 T2,5 780 and one 6 T2,5 160 from CONTITECH. They have the same characteristics as the previously installed belts, which can be seen in *figure 21*.

One very important parameter for the control of the system will be the correlation between steps taken from the motor and the distance travelled by the actuated system. Since the motors that are used have a minimum step angle of 1,8° the minimum movement that can be imposed on the system needs to be calculated as:

$$\theta_{step} = \frac{1.8}{360} 2\pi \approx 0.03142 rad \tag{1}$$

$$D_{pulley} = \frac{zp}{\pi} \approx 12.732 mm \tag{2}$$

Where θ_{step} is the step angle in radiant. D_{pulley} is the diameter of the pulley in millimetres and is calculated with z which is the number of teeth in the pulley and p is the toothed belt pitch in millimetres. It is now possible to calculate the movement caused by one step of the motor by using the equation:

$$l_{step} = \frac{D_{pulley}}{2} \theta_{step} = 0.2 mm \tag{3}$$

The movement can be calculated to be 0.2mm, which is under the set requirement of 0.5mm. Since NEMA 17 motors as the ones used in this application have an uncertainty of about 5% the uncertainty on the position of the actuated system is 0.01mm. Which is abundantly under the capability of measurement of the tracking mechanism that is going to be used.

3.2.6 Control Boards

The main component through which the control of the system is achieved is a Raspberry Pi 3B (*figure 22*). The Raspberry Pi is a single board computer which runs on an operating system based on the Debian GNU/Linux distribution. It distinguishes itself from usual computer boards for its compactness and has the peculiar feature of providing a set of general-purpose input/output (GPIO) pins. This enables interfacing with different types of systems and sensors while also providing 5V and 3.3V output that can be used to supply the low-power components such as the end-stops that are employed in the designed system. Furthermore, the Raspberry can be interfaced remotely through a local Wi-Fi network through the use of SSH protocol. This makes interfacing with the

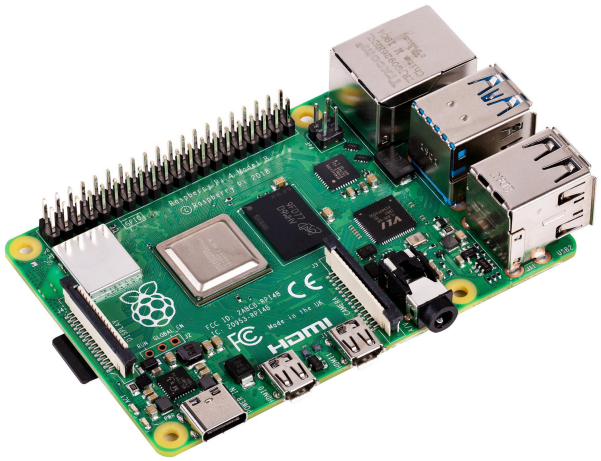

Figure 22: Raspberry 3B used to control the system

system considerably easier as the operator can be seated at one of the laboratory stations while reviewing the data collected by the tracking mechanism. Even though the Raspberry is powered through an external power supply the current and the power that can be delivered to components is limited, it is therefore necessary to use an auxiliary board for powering the most demanding components (i.e. the motors).

This is achieved through the use of an Adafruit DC & stepper motor HAT shown in *figure 23*. This board provides an onboard PWM chip, 4 TB6612 H-bridges and can be stacked with multiple motor HAT to control more than two motors. This is possible if pass-through GPIO pins are connected to the board so that the connection interface to the Raspberry Pi is available for both of them. The presence of these H bridges makes the control of the stepper motor very simple and the algorithm for control is provided on the official Adafruit site. This base algorithm is used as a base for a custom toolbox for motor control. The functional scheme of an H-bridge is present in *figure 23*, by enabling switches 1 and 4 simultaneously the motor is powered and turns in one direction, if switches 3 and 2 are enabled the motor is also powered but turns the opposite direction. The two switches represented are usually MOSFETs due to the high amount of current that runs through them. Stepper motors require 2 H-bridges each because each pole

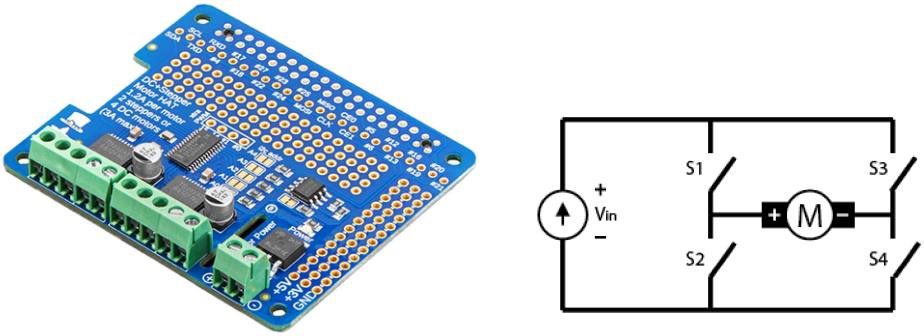

Figure 23: Adafruit motor HAT and H-bridge

winding needs one to be powered in its positive or negative state. The Adafruit motor HAT is connected to the Raspberry Pi with the GPIO interface. A set of pass-through pins are soldered to the motor HAT making communication between two boards possible through the use of I2C protocol while still giving access to the full GPIO interface.

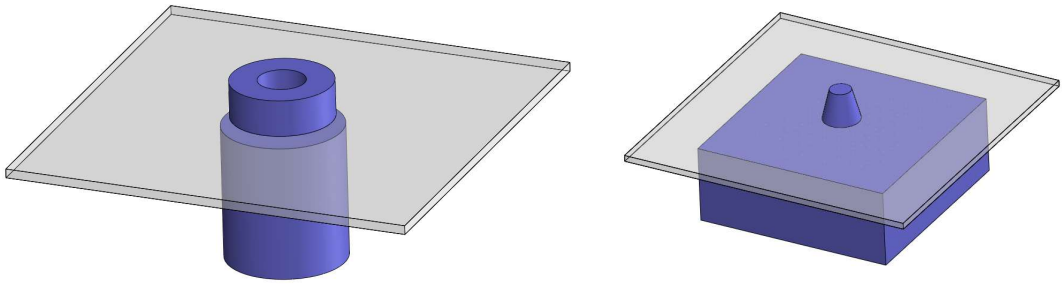

Figure 24: Coarse representation of DOCKS-A and DOCKS-B and their volume

3.3 Design of additional components

This section introduces the additional components designed in order for the kinematics test system to be operable. The following paragraphs will, in fact, explain and justify the shape and functionality of each component. Once the design of these components was completed they were manufactured in two ways: through fused filament fabrication, or through milling of polycarbonate plates to the desired shape. These methods of manufacturing the components have been chosen for ease of prototyping and because the expected loads applied to components are limited. The elements present in the following figures are red if manufactured with an additive manufacturing with PLA plastic or transparent if produced with the mill by cutting polycarbonate plates to the designed specifications.

Before the design of all the necessary components could take place a complete drawing of the pre-existing structure (*figure 14*) was created. Furthermore, a rough CAD representation of DOCKS-A and DOCKS-B has been created to act as a reference for the expected size of mechanisms and systems that this facility is going to test (*figure 24*). These models are used together to check for critical geometric features such as the correct alignment of the connection points between the belts and structure and to check that the tested mechanism fits inside the facility.

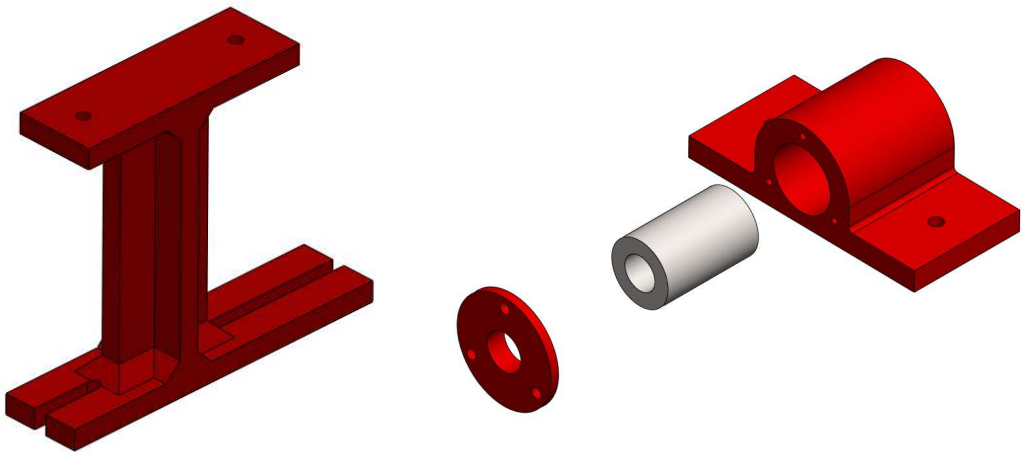

Figure 25: Sliding component, linear bearing representation, bearing blocker and support component

3.3.1 Upper segment design

The upper segment of the system must move along both the x and y-axis. The structural sleds already manage the y-movement; however, a new system for the x-axis movement has to be designed. The main constraints for this system are as follows: (1) compatibility with the available linear bearings; (2) capability to withstand the load that derives from the DOCKS-A assembly being mounted on it, and the contact loads during tests; (3) compactness. In particular, the latter is required by the component for two reasons: for it to fit in the space available between the two guidance rods, and to leave as much workspace as possible beneath it for the tested components. In this design, it is assumed that the tested mechanism is mounted on a plate that is not provided by the testing facility. The final design for the upper segment is quite simple, as it features only two main components:

- a sliding component (*figure 25*), whose task is to house the bearing while securing it;
- a support component (*figure 25*), whose tasks are to provide multiple possible

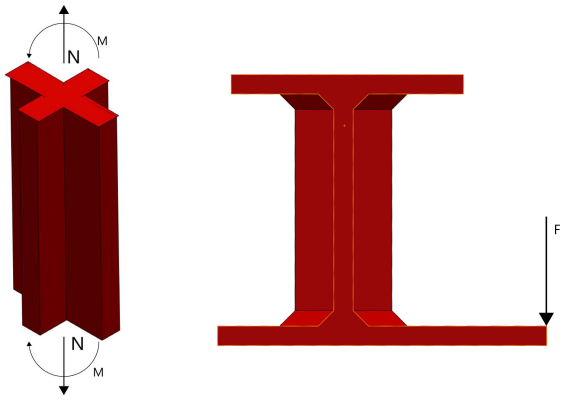

Figure 26: Critical load configurations on the model

anchoring points to mount the plate connected to the tested mechanism and to leave a sufficient amount of space for all the components and system of the tested mechanism between the guidance rods and the support for the tested mechanism.

The sliding component has been designed with a hole of 15,1 mm that houses the linear bearing of 15mm diameter, the extra tenth of a millimetre takes into account the shrinkage that the component is subject to due to thermal contraction since the part will be 3D printed. In fact the print happens on a heated bed at the temperature of 60°C and compounded with any printing error the print may be subject to may cause the produced holes to be to small for the bearing. Both components must be checked for their mechanical characteristics since they are going to be mainly subject to flexural and tension loads, which are critical for structural integrity.

During this evaluation, a maximum load of 2kg is going to be assumed perfectly centred between all the supporting elements. This way the assumption that the load will be equally distributed on all the supporting elements may be considered valid. The segments that are going to be considered are chosen for their potential criticality (*figure 26*):

- the longer support segment for anchoring to the plate, assuming the anchoring screw that supports all the load is on the tip of the support;

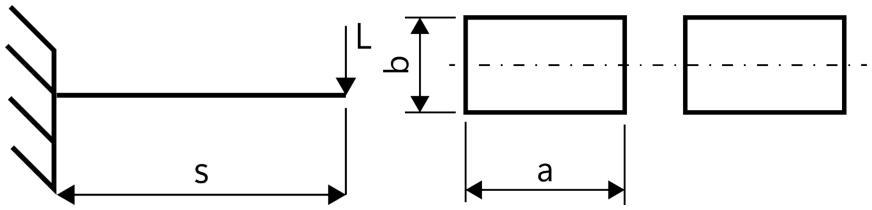

Figure 27: Load configuration and cross-section in the first case

- the vertical section of the support, subjected to simple traction and torque.

While this analysis will consider the material as homogeneous and isotropic this condition does not present in reality. This is due to the nature of 3D printed components, and to the way that 3D printers work in general. Although the matter is complex, for the purpose of this thesis it can be summed up as follows: every 3D-printed item is made of a series of layers, themselves made of fibres; the cohesion between these fibres is stronger inside the layer than it is between different layers. Estimating the strength of 3D printing is extremely difficult, currently a subject of research and is impossible without the use of finite element analysis algorithms. As such, this is only going to be an extremely preliminary evaluation, since it is expected that the designed elements should be capable of supporting the applied loads. Considering this a total safety coefficient of 10 is going to be applied to calculations just to prove their capability of withstanding said loads. Taking into consideration the first case, the mechanical configuration and cross-section of the considered element can be seen in *figure 27*. The maximum bending moment that the load can apply on the section is:

$$L = \frac{m}{4}g$$

$$M = Lz$$

Where g is $9.81\frac{m}{s^2}$, from the first equation L can be calculated to be 4.91N, and given z =41mm, it is possible to calculate M =201.11Nmm The necessary section parameter

for the calculation can be calculated as:

$$I_{xx} = 2\left(\frac{ab^3}{12} - \frac{(a-2t)(b-2t)^3}{12}\right)$$

Given $a = 8.4$mm $b = 5$mm and t is the thickness of the outer shell of the material of 1.2mm, with these parameters it is possible to calculate the maximum tensile and compressive stress present in the considered segment of the component through the use of the formula found in Lenci's book [12]:

$$\sigma_y = \frac{My}{I_{xx}}$$

From which the stress σ_y results to be of 3.19MPa. Even when considering a factor of safety of 10 the minimum tensile strength required from the material would be 31.94MPa, which is still below the average strength of PLA plastic that ranges from 39.9MPa to 52.5MPa as verified in [11].

The calculation for the second condition is a bit more complex since it is a case with both traction and a bending moment applied to the section. The section is the one shown in *figure 28* and the parameters that must be calculated are the area and the second moment of inertia. This can be achieved through the formulas:

$$A_s = 2t\left[2(a-t) + 2(d-t) + 2(e-t)\right]$$

$$I = 2\left(\frac{ta^3}{12}\right) + 4\left(\frac{(d-2t)t^3}{12} + (d-2t)t(a/2)^2\right) + 2\left(\frac{te^3}{12} + te(a/2+e/2)^2\right) + ...$$

$$... + 4\left(\frac{at^3}{12} + (a-2t)t(b/2)^2\right)$$

Given that t=1.2mm, a=5mm, d7.5mm, e=10mm and b =25mm the cross-sectional area of the considered element is A_s=45.36mm^2 while the second moment of inertia is I=4356.69mm^4. Assuming the same load configuration mentioned before, the sec-

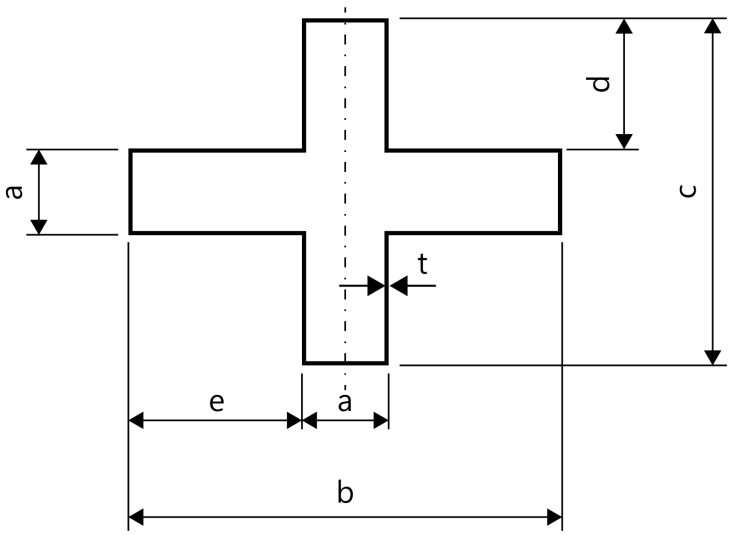

Figure 28: Cross section of the second case

tion will be subject to a traction load of L=4.91N and to a bending moment of $M = Ls = 257.51$Nmm where s=52.5mm. It is therefore possible to evaluate the stresses due to the two loads with the equations:

$$\sigma_z = \frac{L}{A_s}$$

$$\sigma_z = \frac{My}{I}$$

From which a stress from the traction of σ_z=0.108MPa and a stress due to bending moments of 0.74MPa. Using the superposition theorem it is possible to calculate the maximum stress that the system can experience, which is σ_z=0.85MPa. Once again applying a safety coefficient of 10 the minimum material strength would need to be 8.48MPa, which is abundantly below the strength that the material can provide. With this, the analysis of mechanical properties of the upper segment of the system can be considered concluded since the load configurations studied are the critical ones and the designed components managed to withstand the expected loads.

3.3.2 Lower segment design

As mentioned, a part of the lower segment of the facility needs to be able to perform free planar movements. This is achieved through the use of ball transfer units shown in *figure 19*. The lower segment of the system needs to (1) house the ball transfer units in a rigid structure, (2) provide a stiff, planar surface that can move on top of the ball transfer units, (3) provide sufficient space to house all the components of the mechanism.

The additional components that were created to satisfy these requirements are:

- a first plate (*figure 29 left*) that provides anchoring points to the ball transfer units and additional components that are going to be described later;
- a second plate(*figure 29 right*), which will provide the surface for the lower segment of the mechanism to slide and anchoring points that will give adaptability to future systems;
- a supporting system similar to the one for the upper mechanism, for the plates on which the tested mechanism is mounted that allows adaptability for future systems.

The first plate needs to be anchored to the lower segment of the structure through 4 M3 screws and washers on the corners of the plate. These holes have a diameter of 8mm, which may be larger than needed because of the uncertainty on the measure of the position of the threaded holes already present on the base structure of the lower segment.

The plate presents 11 more holes, the 5 central ones are anchoring points for the ball transfer units. The units will be anchored to the plate with the use of two threaded nuts each (one on either side of the plate). This is possible because the ball transfer units present a threaded bolt as a connection interface. This allows for adjustments to the height of each unit individually. Moreover, through this, the inclination of the suspended plate can be adjusted if it slides on its own because of the unevenness of the floor on

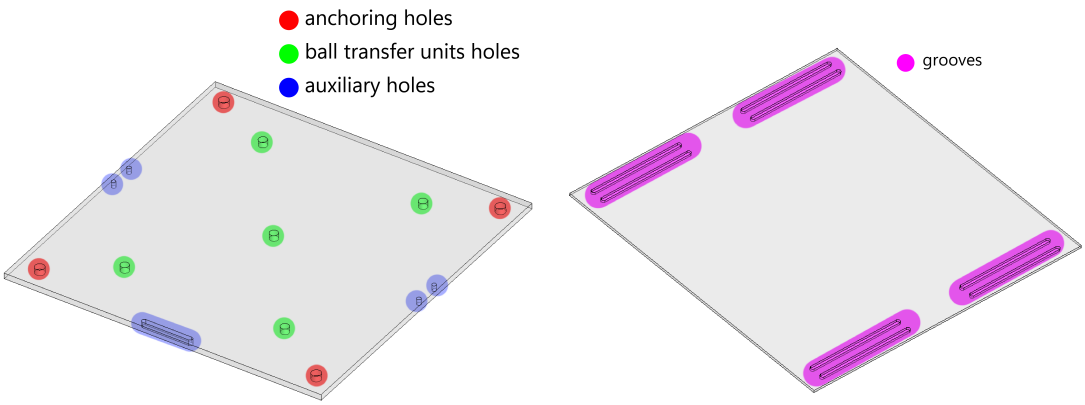

Figure 29: Lower plate for anchoring of components (left) and suspended plate (right)

which the facility might have been laid. The last six holes are present for the anchoring of components that are going to be discussed later in this section.

The second plate is predominantly featureless aside from eight grooves. The lack of features is necessary for this plate to freely slide on the plane defined by the position of the transfer units. If any central feature was present on the plate one of the transfer units might get jammed in it, causing the system to cease to work or even get damaged. These groves provide anchoring points for the supports that are going to be discussed later. They are fairly long to provide the possibility of moving the connection points of the supports to meet the requirement of adaptability to different types of mechanisms.

The design for these supports is quite straightforward: their only task is to provide higher connection points to the plate that houses part of the tested mechanism. The supports are mainly subject to compression and to very small amounts of bending moments. They are connected to the moving plate with two M3 screws on their lower part and to the tested mechanism's plate with one M3 screw on their uppermost part. The combination of the suspended plate and the supporting components creates the possibility of connecting mechanical component plates that range from 100x100mm to 250x250mm as seen in *figure 29*. Potentially even more complex plate configurations can be supported as long as some through holes are reachable by the supporting structure.

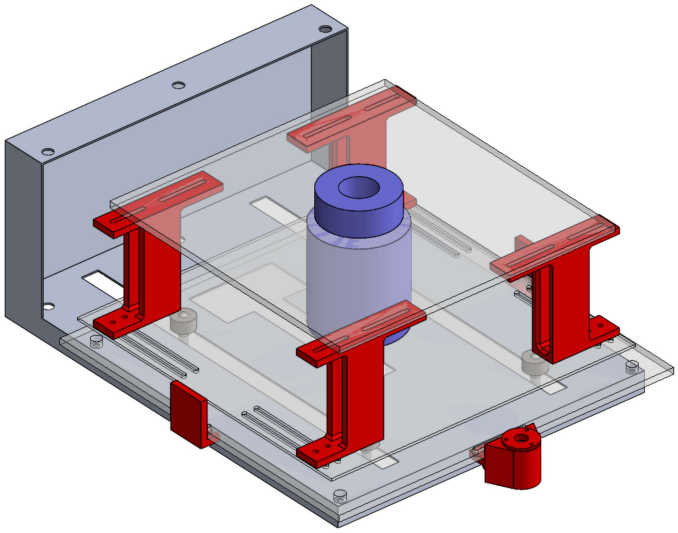

Figure 30: Lower system segment assembly

The other components that connect to the lower plate mentioned before are three. Two of them are just safety elements (they can be seen in *figure 30*) that prevent the suspended plate from moving beyond the support of the ball transfer units and falling outside the structure, potentially damaging both the tested mechanism and the facility. The other component requires its own section to be discussed.

3.3.3 Additional guidance element

In this subsection, the rigidity of the lower segment of the system will be discussed. This is necessary because while the structure of the lower plate could be considered sufficiently rigid for operations in which no loads are present, the same cannot be said for the application the system is being designed for. This is because even small loads on the plate may cause it to deflect and create errors in the measurement of the tested mechanism mounted on it. Considering a load of 2kg on the structural plate it is possible to estimate the amount of the deformation the plate is subject to. Ignoring the weight of the plate and assuming the load applied in the middle in a configuration similar to *figure*

Figure 31: Section of the support plate

27 (the load is applied to the midpoint of the bar) it is possible to calculate the deflection at the furthest point from the fixed extremity while considering the structure as a beam of section represented in *figure 31*. The generic formula to evaluate the deformation of a fixed beam with a load applied to a generic point is:

$$\delta_{max} = \frac{Pa^2(3L - a)}{6EI}$$

This equation can be adapted to our case by substituting P=L, a=$\frac{s}{2}$ and L=s. With this substitution and some simple calculation, the equation becomes:

$$\delta_{max} = \frac{L\frac{5}{8}s^3}{6EI}$$

It is now required to calculate the centroid of the cross-section, which will be on its axis of symmetry. To do so it is possible to use the formula:

$$y_c = \frac{\Sigma y_{ci} A_i}{\Sigma A_i}$$

Taking as reference the lowest left corner of the section the position of the centroid can be calculated to be at y_c=14.92mm. To calculate the moment of inertia of the plate we can use the formula:

$$I = 2\left[\frac{t(h-t)^3}{12} + t(h-t)\left(y_c - \frac{h-t}{2}\right)^2\right] + \frac{at^3}{12} + at\left(h - y_c - \frac{t}{2}\right)^2$$

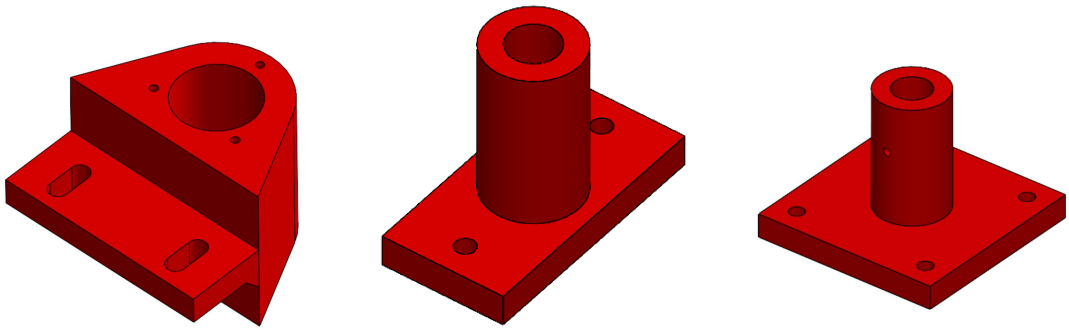

Figure 32: Sliding component and designed supports for the additional guidance rod

Which knowing that h=16.2mm, t=1.2mm a=328mm gives the result I=2886.26mm^4. Using this result in the first equation written in this subsection, considering that the length of the beam considered is one of the plates of s=304mm and assuming Young's modulus for aluminium of 68MPa, it is finally possible to calculate the maximum deflection of the plate which results in δ_{max}=1.76mm.

The calculated deflection is considerable but the estimation that has just been conducted is imprecise. The actual deformation is even greater since the calculation does not take into consideration the presence of slots along the center plate, which degrade the plate rigidity. From this considerations it becomes clear that the design of some method to increase the rigidity of the lower segment of the system is required.

To improve the rigidity the component mentioned in the last section will be utilized. It is conceptually similar in design to the sliding components mentioned in the previous subsection but its task is different. This component houses bearing and is connected to an additional guidance rod that is on the other side of the supporting structure of the lower segment of the system. The addition of this guidance rod does not provide any load bearing capability but it is meant to increase rigidity. The effect of the presence of this component that slides along the guidance rod on the supporting structure is to deny the rotation around the x-axis of its extremity. This should provide additional rigidity to the system without impacting it in any way, as long as the new guidance rod is mounted

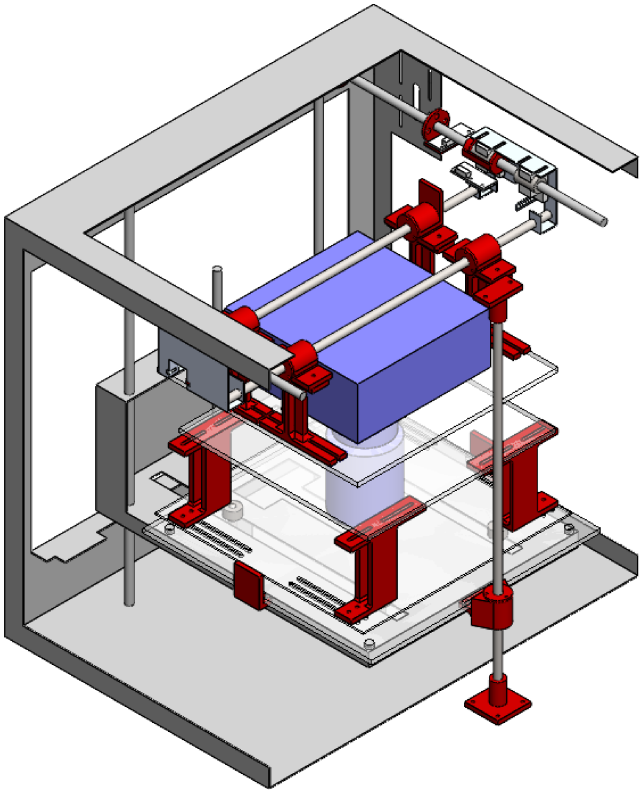

Figure 33: CAD representation of the complete assembly

perfectly parallel to the ones that are already present.

The elements that anchor this guidance rod to the main structure of the system were the last to be designed (*figure 32*). These two components are similar to each other and are composed of one base plate with two or four through holes to anchor them to the external structure with M3 screws. They also present an empty cylindrical element that has the task of housing a portion of the guidance rod to indirectly connect it to the external structure.

3.4 System control

3.4.1 Programming language and interfacing

The main objective of the control of the system is fairly simple: to impose a known misalignment to the upper part of the system during manoeuvres and keep track of the position of both the upper and lower segments of the tested mechanism through the use of the open loop control of the stepper motors and the infrared tracker. All of this to verify that the tested mechanism can tolerate the misalignments that have been previously verified with virtual simulations. To manage the position, the stepper motors are controlled in micro-stepping mode through programs designed in MATLAB & Simulink. The first one is written in MATLAB: it is a program that contains all the necessary parameters for the Simulink script, such as the movement-motor rotation correlation, the simulation step time, the distances that the motor needs to travel, etc.

The Simulink program was designed with Raspberry Pi compatibility in mind, as such input and output blocks belonging to a custom blocks library were used. Part of the code in the Simulink blocks makes interfacing with the Raspberry Pi GPIO and Adafruit motor HAT a lot simpler. Furthermore, Simulink presents an auto-coding feature that enables the "translation" between the MATLAB& Simulink programming language to one that can be read and run on the Raspberry Pi.

The main custom blocks that are used in the program are the GPIO read and Adafruit motor HAT control. The first block reads the state of one pin on the Raspberry Pi and is used for reading the end-stop switch signal and user inputs. The second block defines the control parameters for the motors, e.g. control mode (micro-stepping, full step etc), RPM and I2C address for the Adafruit board. This block takes as input an enabling signal and the number of steps that the motor needs to take, this number can be positive for a clockwise rotation and negative for a counter-clockwise rotation.

One peculiarity of the motor control block is that it is "blocking", meaning that if the

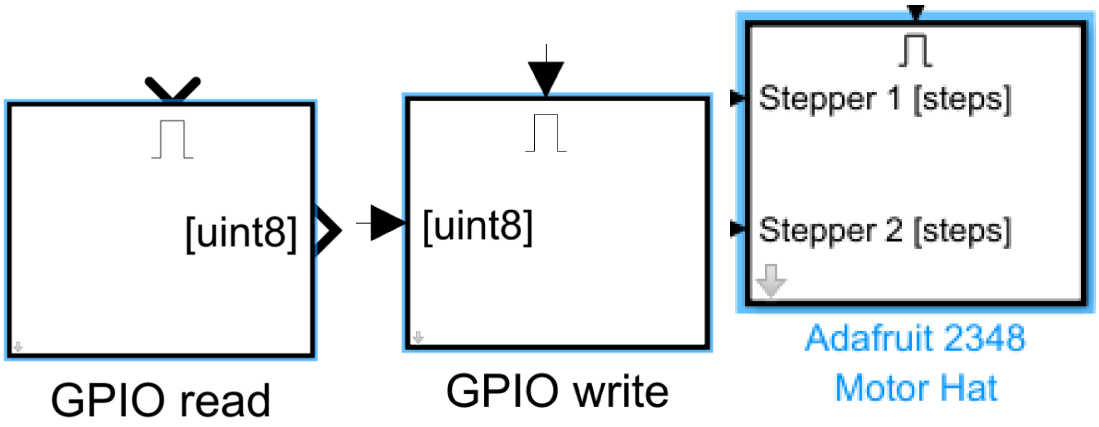

Figure 34: Blocks to interface with the Raspberry Pi GPIO and stepper motors

number of steps that the motor is commanded to take is bigger than the number that can be taken in the time step of the simulation, which will halt and wait for the command to be completed. This is problematic especially during the homing procedure as the sensors would only be read once at the beginning of the manoeuvre instead of being polled for the duration of the whole manoeuvre. This issue has been resolved by feeding the motor control block with a singular step input. With this as long as the simulation step time is bigger than the time necessary to take a step the command never goes to the blocking condition. This solution introduces another problem: the coupling of the speed motor and the simulation time step. However, this solution is still an acceptable compromise, since the test does not require high speeds and the testing procedure is not particularly long. Furthermore, this control method introduces the need for a "counter" system that counts the number of steps taken from the beginning of the manoeuvre. This is simply resolved by counting the amount of time a single stateflow block is activated 2(*figure 35*).

3.4.2 Control phases

The control of the system as a whole depends on the tests that need to be performed. Therefore, the test procedure must be defined for a functional program to be built. For

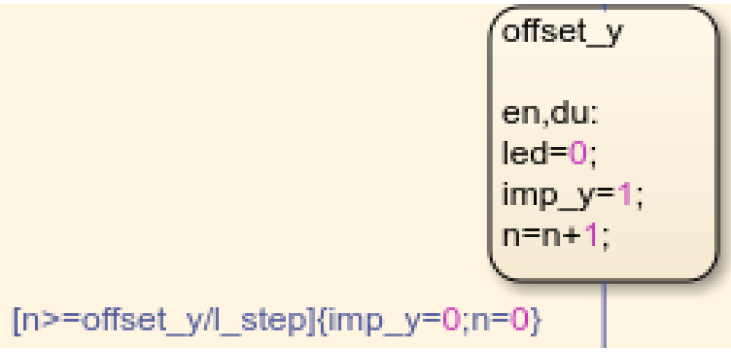

Figure 35: Stateflow block that counts the steps and the next phase condition

the procedure, it is possible to take inspiration from section 2.3 where similar procedures were conducted.

The test procedure follows the following steps:

1. HOMING: during which the motors move the controlled part of the tested mechanism at the edge of its workspace, this is done to provide a known starting point for the control of the stepper motors;

2. CENTERING: during which the controlled system is moved to the center of the available workspace to provide the maximum possible space for testing;

3. CALIBRATION: during which the lower segment of the tested mechanism is brought into contact with the upper segment;

4. TEST PREPARATION: during which the two segments of the tested mechanism are separated and brought to their starting position;

5. OFFSETTING: during which only the upper segment of the system is moved to provide the desired geometric testing conditions. In some cases this might require the manual introduction of a rotation around the z-axis;

6. TESTING: the upper and lower segments of the tested mechanism are brought into contact once again, verifying if a correct docking procedure can take place

with the applied offset;

7. RESETTING: after all the necessary measurements have been taken the upper part of the mechanism is brought to the centre position, displacing the lower suspended segment along with it (in the x and y-axis);

8. PARAMETERS MODIFICATION: after the resetting step all the motor step counters are reset to zero and a new offset parameter is applied, the control logic is returned to the test preparation phase for further testing.

Depending on the success of the test the new offset applied to the tested mechanism varies with the following logic: if the test is successful the offset is increased by a fixed amount for every iteration, if the test run fails the offset is decreased by half of the pre-defined amount. This procedure is repeated until the maximum acceptable misalignment is found. The test procedure is considered a success only in the case of successful interlocking of the two tested geometries.

All of the phases present in the program are described inside a stateflow block provided by a library. The use of stateflow allows for simpler control of the system and activation of subsequent phases. While each of these control phases have a dedicated Simulink stateflow control block, most of them are similar in design. They deliver a certain amount of impulses to the driven motor that represents the number of steps that need to be taken. The amount of steps is calculated in the initialization MATLAB script for manoeuvres that are always the same, such as centering and calibration, but are also calculated while the script is running, e.g. during the offsetting phase. This is the equation used for the calculation:

$$n_{steps} = \frac{L}{l_{step}}$$

where L is the wanted movement and l_{step} is the amount of movement caused by a single motor step calculated in section 3.2.5 The amount of steps taken is counted during the

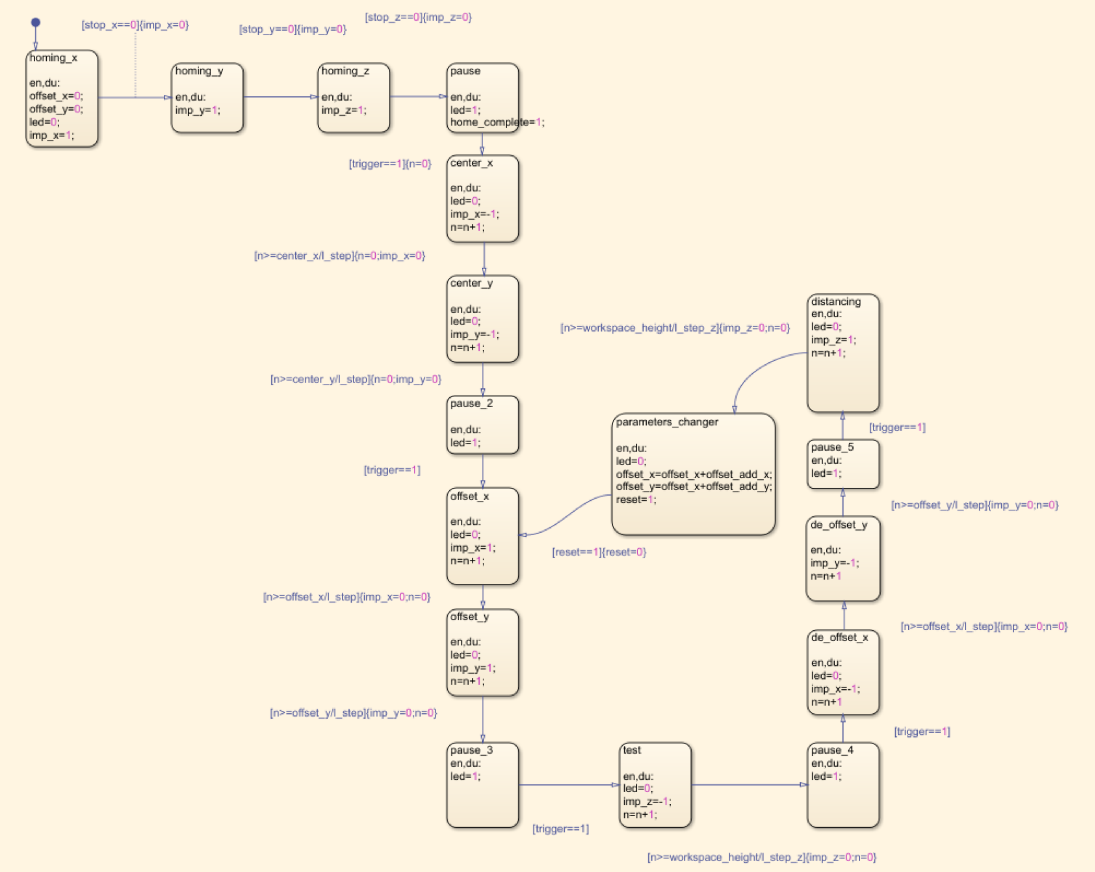

Figure 36: All the stateflow phases and their activation

execution of the script and is used as a stop parameter for the command. The only Simulink block that is dissimilar from the others is the one that controls the homing phase. In fact, its working logic is different, instead of using a step counter to stop the manoeuvre it uses the signal from the end-stop switches to cease the motor rotation since it means the homing procedure is completed.

The switching between phases is achieved though stateflow conditions such as reaching the required amount of steps or end-stop activation. An additional stateflow phase is added between the main phases, it is a pause phase in which the program waits for a user input through the use of a button. Once the pause button is pressed the program proceeds with the next phase. The entire stateflow logic can be seen in *figure*

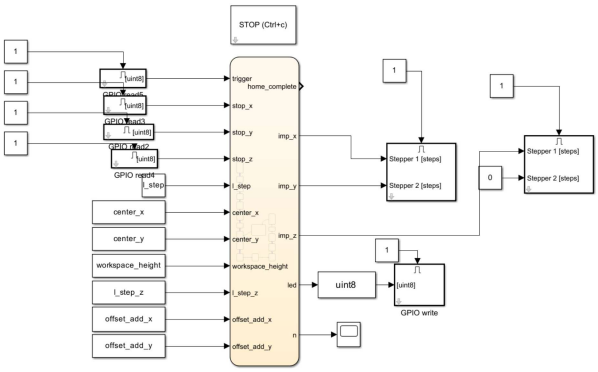

Figure 37: Scheme of the entire Simulink code

Figure 38: infrared cameras and infrared refractors used in the facility

36 and the complete Simulink program can be seen in *figure 37*.

3.4.3 Motion tracking system

The set of infrared cameras that are going to be used to keep track of the two segments of the tested mechanism are 4 OptiTrack Prime^{x}13 (*figure 38*). Each of these cameras work by emitting infrared light and then capturing the position of various reflective markers. Each of the cameras collects data on the position of the marker on the sensor (*figure 38*) and by knowing the relative position of each camera it is possible to calculate the absolute position of the marker. If more than 3 markers are visible to each sensor a further calculation on the attitude of the object on which the markers are applied.

Since a direct line of sight from the camera to the reflective marker is needed for the

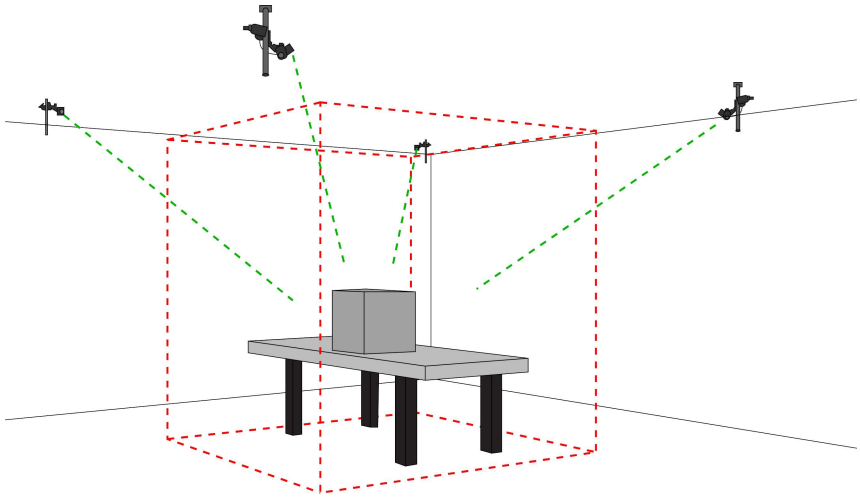

Figure 39: Tracking setup

position and attitude estimation of the marker to be calculated some supports need to be introduced. They will only act as connection points for the markers and are different based on the mechanism that is going to be tested. Ideally, all of the cameras should be able to "see" the marker to achieve optimal tracking but the system can operate with one camera occluded. To achieve the best camera coverage the marker should protrude out of the facility structure by some centimetre to achieve optimal visibility. While this is possible for the part of the mechanism that is connected to the upper segment of the testing facility the same is not valid for the other part. Consequently, the tracker connected to the lower part of the mechanism protrudes laterally from the structure. Unfortunately, this makes it impossible for all 4 cameras to have a direct line of sight to the marker of the lower tested mechanism but a smart positioning in the facility in the tracked space can achieve a constant line of sight with three cameras, thus allowing continuous tracking of both of the tested mechanism elements (*figure 39*).

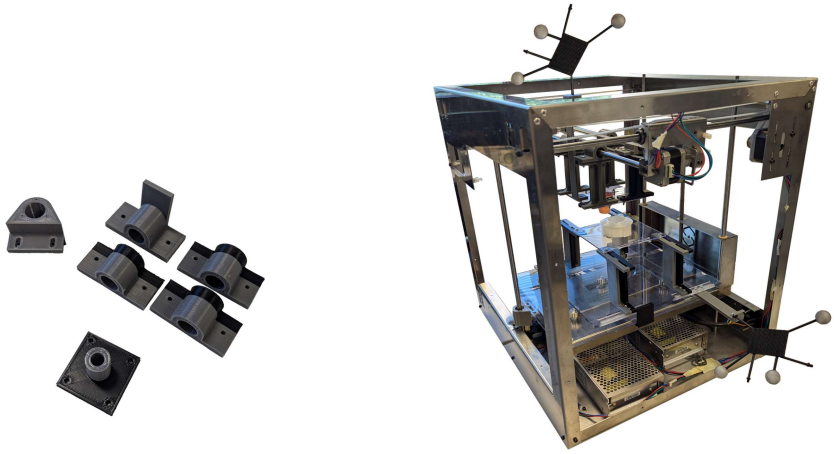

Figure 40: Some of the printed and machined elements, complete system assembly

4 Final assembly and testing

During the assembly of the system, it became apparent that the holes that should hold the bearings or rods were too small even though during the design phase the thermal contraction phenomena had already been accounted for and the holes were thus oversized to begin with. This is because filament 3D printing can be, at times, imprecise as a manufacturing method due to a large number of uncontrollable variables, such as variations of the filament diameter which can cause the holes to be either bigger or smaller than anticipated. As such, two cylinders with pass-through holes and variable diameters were designed to find out not only the actual size of the printed holes but also the correct measurements for the new prints to finally be effective. These calibration cylinders change diameter along their length in steps of 0.1mm between 8.1mm and 8.7mm for the 8mm hole, and 15.1mm and 15.7mm for the 15mm hole. The correct measurements found were, respectively, 8.3mm and 15.4mm. Cylinders of these measurements slide into the holes with a good amount of friction between the component enclosure and the mechanical element they are supposed to hold, be it a rod or a bearing.

Once the adjustments on the internal diameters on the necessary components were

applied they were re-printed. The necessary plates were machined and the result can be seen in *figure 40*. These components were assembled as designed and explained in section 3.3 and the final result can be seen in *figure 40* (right). The markers mentioned in the previous section are then applied to each of the plate of the tested mechanisms, while making sure that at least 3 cameras have direct line of sight when placing said markers.

Once all the components, sensors and motors are mounted with DOCKS-A and B as the tested mechanism, a preliminary test can be conducted to verify the correct operation of both the facility and the tracking system. To do so, the markers are also mounted on DOCKS-A and B and the entire system is placed into the trackable workspace between the tracking cameras as seen in *figure 39*. The bolt transfer units are calibrated to compensate for the local height difference (that of the testing room floor).

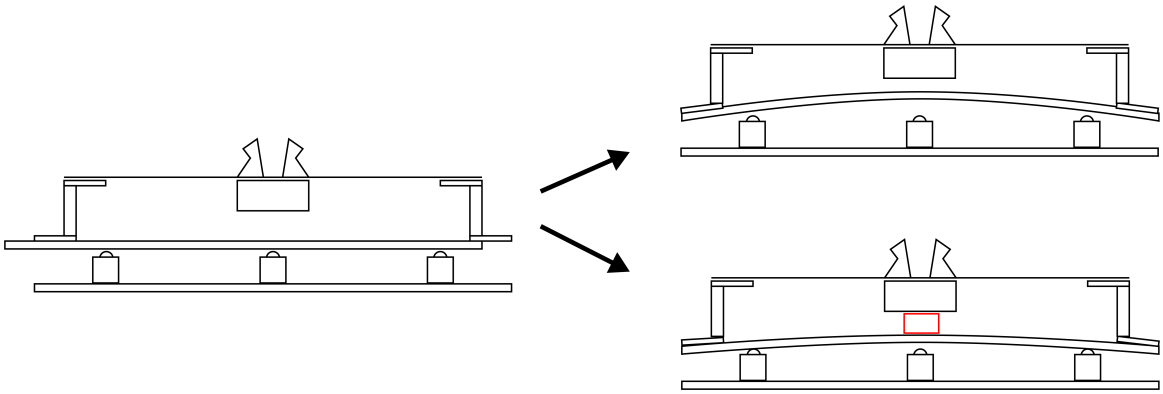

Figure 41: Suspended plate desired configuration, deformed configuration, mitigated configuration

5 Conclusions

As the project ends, conclusions can be drawn. As discussed, the objective of the thesis was to create a facility for the kinematic testing of small docking mechanisms while providing adaptability of use for future testing campaigns. This is because the pre-existing testing facilities available at the Space Systems Laboratory at Università degli Studi di Padova are slow to operate, although they do have their advantages, such as a higher amount of DoF and a bigger testing workspace. It might be useful to sum up the steps followed during the project before drawing the conclusions. At first, requisites were defined; pre-existing facilities were studied to inspire the design, and a State of the Art section was compiled; finally, in this first part, options were considered for the free movement allowed to the suspended plate. Then, the components were designed; they were evaluated in strength and stiffness where needed; and a control system was implemented. Lastly, everything was either printed with a filament 3D printer or milled out of polycarbonate, and tests were conducted. The results of these test are visible in *figure 43*.

Some considerations can now be made. All the imposed requirements have been met but some further improvements on the system can be made. One of such improve-

ments can be replacing the suspended plate for an aluminium or steel one. Although this has a considerable effect on the mass and inertia of the system, the additional rigidity that the aluminium plate provides might be necessary, especially when testing heavier mechanisms. This is because although the poly-carbonate plate is 5mm thick and provides a fair amount of rigidity, in the considered configuration the load is concentrated on the sides of the panel. This load configuration may cause the suspended plate to become convex, causing the lower part of the system to be unable to freely move in the plane as required. The current system can still be considered functional but the weight of the segment of the tested mechanism that is mounted on the lower plate must be taken into consideration before the testing procedure. This behaviour might be mitigated by adding an element between the suspended plate and the tested mechanism. This additional element transmits part of the load between the tested mechanism and the center of the plate, reducing its deformation. This behaviour can be observed in *figure 41*.

Another possible improvement might the reintroduction of one of the degrees of freedom that were discarded at the beginning of the design phase. This may be achieved with the use of an additional guidance rod parallel to the x direction one (*figure 42*). This additional rod will act as the axis of rotation for some additional supports that can be connected to the plate of the tested mechanism. This allows the plate on the upper segment to spin and adapt to any inclination that may be imposed to the lower mechanism by the addition of a spacer on the plate's anchoring point. In the case the system is asymmetric two separate tests can be conducted to evaluate how the system manages pitch and yaw misalignments. Unfortunately, this was not possible in the current set up due to the size of the system. In fact, with the addition of the rod system occupying space next to the upper plate there would not be sufficient space between the two sides of the mechanism anymore to allow for the full retraction of the probe outside the drogue, which would make proper testing procedure impossible to conduct. This, however, is not an issue when testing mechanisms and systems of smaller size, and can consequently

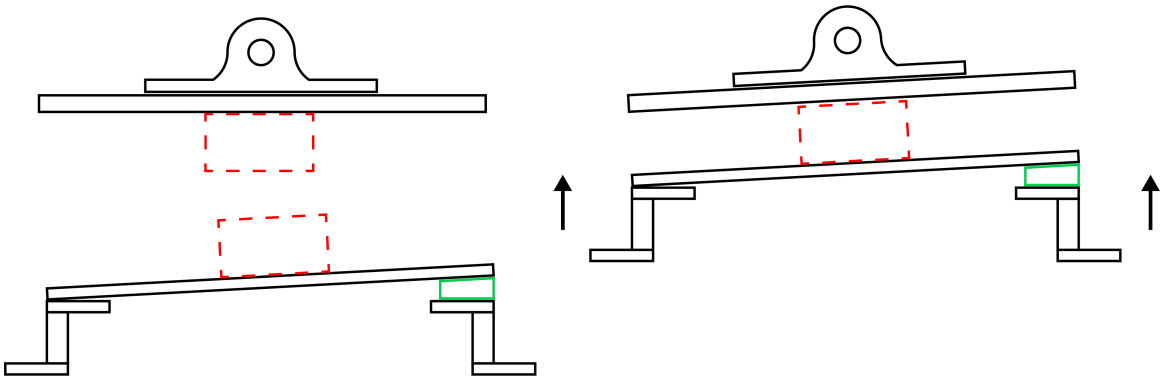

Figure 42: Configuration that allows for yaw misalignment testing conceptual scheme

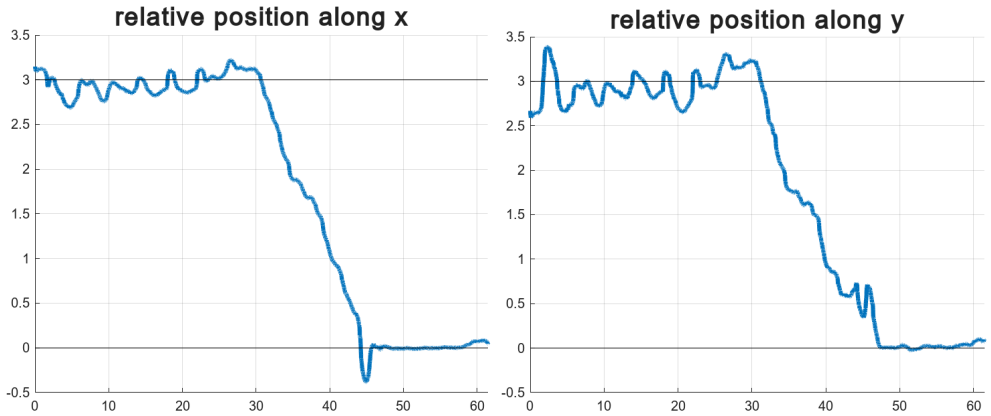

Figure 43: Test results acquired with the tracking system with a starting offset of 3mm along both x and y

be implemented in the future as the requirement to test such a system arises.

One last useful addition to the system might be a load cell mounted on one of the supports of either the higher or lower segment. This cell would act as a stop signal during testing phases and could be used as both a success or failure signal depending on when the cell is activated.

In conclusion, the assembled facility meets the imposed requirements, and although some improvements are possible, its performance can be considered sufficient for the current application, and the work can be considered overall successful.

List of Figures

Bibliography

[1] Jennifer D. Mitchell et al. “Automated Rendezvous and Docking Sensor Testing at the Flight Robotics Laboratory”. In: (2007), pp. 1–16. DOI: 10.1109/AERO.2007.352723.

[2] Swati Mohan et al. “SPHERES flight operations testing and execution”. In: *Acta Astronautica* 65.7 (2009), pp. 1121–1132. ISSN: 0094-5765. DOI: https://doi.org/10.1016/j.actaastro.2009.03.039. URL: https://www.sciencedirect.com/science/article/pii/S0094576509001726.

[3] Hans Krüger and Stephan Theil. “TRON - Hardware-in-the-Loop Test Facility for Lunar Descent and Landing Optical Navigation”. In: *IFAC Proceedings Volumes* 43.15 (2010). 18th IFAC Symposium on Automatic Control in Aerospace, pp. 265–270. ISSN: 1474-6670. DOI: https://doi.org/10.3182/20100906-5-JP-2022.00046. URL: https://www.sciencedirect.com/science/article/pii/S1474667015318516.

[4] Stephen Calrk. “Spaceflight Now: Juno Spacecraft Set to Begin Epic Journey”. In: (2011). URL: https://spaceflightnow.com/news/n1104/07junotrailer/.

[5] Zaber Technologies. *Microstepping Tutorial*. 2014. URL: https://www.zaber.com/articles/microstepping-tutorial.

[6] OPTIBELT. *Technical Data Sheet optibelt ALPHA TORQUE T2.5 - ST PU Timing Belt, Cast Polyurethane, Endless*. 2015. URL: https://docs.rs-online.com/6efa/A700000007539081.pdf.

[7] Bill Drury Austin Hughes. *Electric Motors and Drives: Fundamentals, Types and Applications*. School of Electronic and Electrical Engineering, University of Leeds: Elsevier Science I& Technology, 2019.

[8] Markus Wilde, Casey Clark, and Marcello Romano. “Historical survey of kinematic and dynamic spacecraft simulators for laboratory experimentation of on-orbit proximity maneuvers”. In: *Progress in Aerospace Sciences* 110 (2019), p. 100552. ISSN: 0376-0421. DOI: https://doi.org/10.1016/j.paerosci.2019.100552. URL: https://www.sciencedirect.com/science/article/pii/S0376042119300466.

[9] Francesco Branz et al. “Miniature docking mechanism for CubeSats”. In: *Acta Astronautica* 176 (2020), pp. 510–519. ISSN: 0094-5765. DOI: https://doi.org/10.1016/j.actaastro.2020.06.042. URL: https://www.sciencedirect.com/science/article/pii/S0094576520304082.

[10] RepRap. *Mechanical Endstop*. 2021. URL: https://reprap.org/wiki/Mechanical_Endstop.

[11] Ge Gao et al. “Study of material color influences on mechanical characteristics of fused deposition modeling parts”. en. In: *Materials (Basel)* 15.19 (Oct. 2022), p. 7039.

[12] S. Lenci. *Lezioni di Meccanica Strutturale*. Società Editrice Esculapio, 2023. ISBN: 9791222091495. URL: https://books.google.it/books?id=lbS3EAAAQBAJ.

[13] Luca Lion et al. “Kinematic tests on a docking mechanism for microsatellites”. In: *CEAS Space Journal* (2023). ISSN: 1868-2510. DOI: 10.1007/s12567-023-00516-w. URL: https://doi.org/10.1007/s12567-023-00516-w.

[14] RS Components. *THX linear guide*. 2024. URL: https://it.rs-online.com/web/p/carrelli-per-guide-lineari/7300023?gb=sp.

Ringrazio la mia ragazza per tutto il supporto che mi ha dato durante la stesura della tesi e i miei genitori per essere sempre stati presenti durante il mio percorso di studi. Ringrazio inoltre il professor Branz che mi ha seguito durante questo progetto.